RESEARCH MEMORANDUM

EVALUATION OF HYDROGEN FUEL IN A FULL-SCALE AFTERBURNER

By Donald E. Groesbeck, William R. Prince, and Carl C. Ciepluch

Lewis Flight Propulsion Laboratory
Cleveland, Ohio

NATIONAL ADVISORY COMMITTEE
FOR AERONAUTICS

WASHINGTON

September 24, 1957

~~CONFIDENTIAL~~

NATIONAL ADVISORY COMMITTEE FOR AERONAUTICS

RESEARCH MEMORANDUM

EVALUATION OF HYDROGEN FUEL IN A FULL-SCALE AFTERBURNER

By Donald E. Groesbeck, William R. Prince, and Carl C. Ciepluch

SUMMARY

A performance investigation using hydrogen fuel in a full-scale afterburner was conducted with particular study of fuel-injector configurations and afterburner length. A total of seven fuel-injector configurations, grouped by type as concentric ring or radial bar, were investigated at a burner-inlet velocity of approximately 600 feet per second over a range of burner-inlet total pressures from 330 to 950 pounds per square foot absolute. Afterburner length was varied from 27 to 69 inches. No flame-stabilizing devices other than the fuel injectors were used.

Data presented indicate that maximum combustion efficiencies at a balanced-cycle condition for a ring-type fuel injector in a 39-inch burner were 94 and 78 percent for burner pressures of 890 and 488 pounds per square foot absolute, respectively. Increase in afterburner equivalence ratio beyond that for peak efficiency resulted in a serious drop-off in combustion efficiency. Variation in fuel-injector variables such as direction of injection, orifice diameter, and fuel-bar diameter did not significantly affect combustion efficiency.

CE-1

INTRODUCTION

Analytical and experimental studies on the use of hydrogen as a fuel in a ramjet, turbojet, simulated afterburner, tubular combustor, or a short engine combustor are reported in references 1 to 9; however, none of these included work on a full-scale afterburner. Therefore, the purpose of this investigation, conducted in an altitude test chamber at the NACA Lewis laboratory, was: (1) to explore the problems associated with using hydrogen in a full-scale afterburner, and (2) to determine the burner-design variables that would be applicable to future hydrogen afterburners. In addition, the range of previous investigations has been extended to simulated altitudes of 90,000 to 100,000 feet and to Mach numbers of 2.0 to 2.5.

The burner-inlet total-pressure range used in the program was from 950 to 330 pounds per square foot absolute. The afterburner was designed

~~CONFIDENTIAL~~

for an average burner-inlet velocity of approximately 600 feet per second. Afterburner variables receiving particular attention were the fuel-injector configurations and the burner length. Because the primary objective of the program was an evaluation of afterburner performance, only general observations were made of operational characteristics such as "shell" cooling and ignition; these observations are summarized briefly.

APPARATUS

Installation

The engine-afterburner combination was installed in an altitude test chamber as shown in figure 1. A bulkhead with a labyrinth seal around the engine-inlet duct was used to allow independent control of inlet and exhaust pressures. The laboratory air systems supplied combustion air to the engine and removed the exhaust gases; the facility thrust system was not used. The investigation was conducted with an axial-flow turbojet engine.

Instrumentation

The location and the amount of instrumentation used in the afterburner are shown in figure 2. A photograph of the water-cooled total-pressure rakes installed at station 9 is shown in figure 3. Engine fuel flow (JP-4) was measured by a calibrated remote-indicating flowmeter. Afterburner fuel flow was measured by a calibrated orifice. All of the pressures were measured by null-type diaphragms recorded by a digital automatic multiple pressure recorder (a modified version of the pressure recorder used in ref. 10). The temperatures were measured with iron-constantan and shielded Chromel-Alumel thermocouples and were recorded by self-balancing potentiometers. Radiation and recovery corrections were applied to all Chromel-Alumel thermocouple readings (ref. 11).

Afterburner Configurations

Afterburner. - Figure 2 illustrates the location of the afterburner components and presents the pertinent dimensions and burner details for the two afterburners used. The two afterburners were the same except that burner A had a solid cooling liner, while burner B had no liner but was externally water-cooled. Liner misalinement between individual burner sections due to warpage led to the use of the water-cooled afterburner configuration during the latter part of the investigation. Both burners consisted of various length spool pieces (capable of being bolted together in any order, thereby varying burner length). The diffuser, incorporating antiwhirl vanes, vortex generators, and a conical inner

body, measured $38\frac{1}{2}$ inches in length from the turbine outlet to the burner inlet. The diffuser configuration was selected for its low whirl and relatively flat velocity profile, as discussed in reference 12. The burner section was cylindrical (29.4-in. diam.) and measured 6 feet from the diffuser exit to the exhaust-nozzle inlet. Afterburner length, herein defined as the distance from the point of fuel injection to the exhaust-nozzle inlet, was varied in burner A by relocating the 6-inch spool piece containing the fuel injectors. Afterburner length for burner B was varied by using the alternate fuel-injector location. No conventional-type flameholder was used in the investigation, since the spray bars were expected to provide any needed flame stabilization. The over-all length of the afterburners from diffuser inlet to exhaust-nozzle outlet was approximately 12 feet and remained fixed for the entire investigation.

Exhaust nozzles. - Four exhaust nozzles having throat areas ranging from 86 to 62 percent of the full-burner area were used in the investigation (fig. 4). The nozzles were constant-area convergent-divergent types that were chosen because of the ability to remain choked at a pressure ratio (nozzle-inlet total pressure to ambient static pressure) of approximately 1.2, as compared with a convergent nozzle requiring the normal choked pressure ratio of approximately 1.9. The convergent-divergent type nozzles were used because of the desire for extremely low burner pressures, together with facility exhaust-pressure limitations and the requirement of choked-exit station in the gas temperature calculations. The throat sections of the nozzles were water-cooled in order to minimize any change in the throat area with heat addition.

CE-1 back

Fuel injectors. - Seven fuel-injector configurations (figs. 5 to 10), grouped by type as either concentric rings or radial bars, were investigated. The pertinent dimensions and details of the fuel injectors are presented in table I.

METHODS AND PROCEDURE

Engine Operation

An axial-flow turbojet engine was used to provide realistic afterburner-inlet conditions; however, JP-4 fuel was burned in the main engine combustor because of the limited supply of hydrogen. The effect of using the two fuels was considered in all applicable calculations. The engine speed was set and automatically maintained by engine fuel-flow modulation. Engine-inlet pressure was adjusted as required to maintain desired burner pressure, and the exhaust pressure was maintained at a value sufficiently low to choke the exhaust nozzle.

[redacted]

Afterburner Operation

The operating envelope that defines the area of the investigation in terms of burner-inlet pressure and afterburner equivalence ratio (defined in appendix B) is shown in the following sketch:

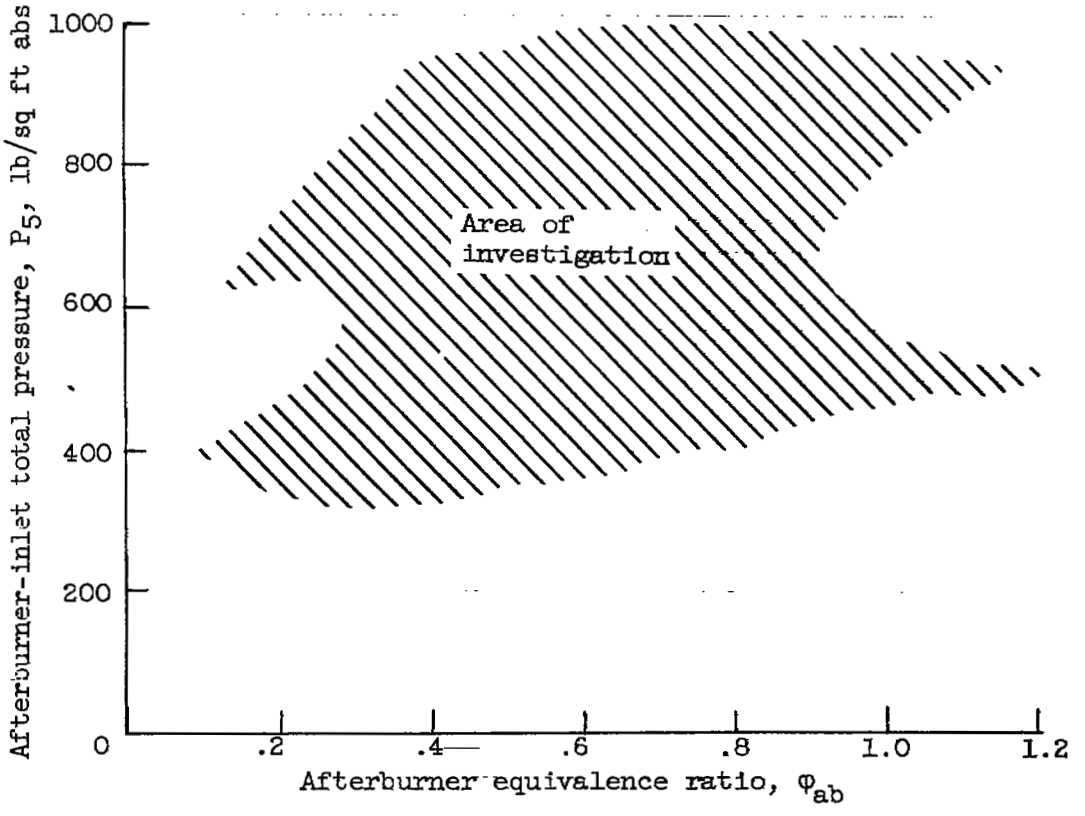

The complete range of operating variables, including burner length, nozzle area, and engine-inlet and burner-inlet pressure for all fuel-injector configurations investigated, is presented in table II.

The afterburner equivalence-ratio range corresponded to a fuel flow producing limiting turbine-outlet gas temperature (approximately 1700° R) either to minimum turbine-outlet temperature (approximately 1300° R), or to lean blowout, whichever occurred first.

The afterburner outer shell, fuel injectors, and combustion zone were observed visually during the investigation by using observation ports and a periscope directed toward the fuel injectors from outside the exhaust nozzle.

The symbols are defined in appendix A and the methods of calculation are presented in appendix B.

RESULTS AND DISCUSSION

The results, in general, are presented in the order in which the tests were conducted, and the discussions evaluate the principles investigated. The severe afterburner velocity levels and inlet-pressure conditions were selected in order to magnify any performance changes resulting from modifications.

Combustion Efficiency, Configuration A

Three sets of efficiency data, representing a general exploration of fuel-injector configuration A (concentric ring-type injector similar to configuration reported in ref. 4), are shown in figure 11. Afterburner pressure level had a considerable effect on efficiency, as noted in figure 11(a) by the 25-point drop in peak values with a decrease in pressure from approximately 900 to 400 pounds per square foot absolute. The occurrence of the peak efficiencies at an equivalence ratio of approximately 0.5 indicates considerable fuel-air stratification in the combustion zone with local zones operating at or near ideal fuel-air mixture, while the other zones may be operating extremely lean or completely void of any fuel at all. Increasing the equivalence ratio beyond that for peak efficiency resulted in over-rich local zone operation and, as a consequence, large losses in efficiency. A cursory comparison of the efficiency values at balanced-cycle conditions (burner-inlet temperature of 1700° R) in parts (a), (b), and (c) of figure 11 may lead to false conclusions because the exhaust-nozzle area is different in each of the three parts, and, since the areas are different, balanced-cycle temperature (1700° R) occurs at vastly different afterburner heat releases. Since the peaks in the curves in figure 11 all occur at approximately 0.5 equivalence ratio, they probably are a function of the injection pattern. Also, the coincidence of the 1700° R temperature and the 0.5 equivalence ratio (fig. 11(a)) resulted in maximum efficiency values, even though the burner length was the shortest investigated.

The conclusion can be made that, for configuration A, the reduction in afterburner pressure severely penalized combustion efficiency and the performance did not meet the objective of high efficiency, especially at fuel flows near stoichiometric fuel-air ratio where maximum thrust output would be achieved.

Design Considerations for Fuel Injectors

Orifice locations for a uniform fuel-air distribution are of increased importance in the absence of turbulence-generating or flame-seating devices, such as flameholders (see table I giving the fuel-injector configurations for orifice distribution). In addition to orifice location, other factors having a possible effect on the fuel-air distribution and thus on the efficiency and stability limits are: (1) injection direction, (2) orifice diameter and fuel penetration, and (3) fuel-bar size. The effects of these variables are discussed in the following paragraphs.

Effect of fuel-injection direction. - Figure 12 shows the effect of fuel-injection direction on afterburner performance at two burner pressure levels. Radial fuel bars (configuration D) were rotated in 45° increments from full upstream to full downstream injection. For the high pressure level, normal injection caused a severe drop in efficiency and stability margin; and, at the lower pressure level, 45° upstream injection resulted in the same effect. From the results shown, it can be concluded that upstream, 45° downstream, and downstream injection cause no detrimental effects on stability characteristics.

Reference 5 reports that 45° downstream injection is a good compromise on performance; this conclusion was based on a flatter efficiency curve over a range of equivalence ratios and on the fact that mild screech was encountered only at certain conditions. A marked difference with injection direction is also reported. However, the conditions covered in reference 5 are not in the range reported herein, so a justifiable comparison cannot be made. It does indicate, however, that additional investigation of fuel-injection direction is needed.

Effect of fuel penetration and injector-orifice diameter. - The use of larger fuel-orifice diameters with consequently lower fuel supply - pressure requirements for a given fuel flow is extremely important from the standpoint of tank weight in an aircraft installation.

Radial bars, injecting fuel upstream, were used in this investigation, and the injector orifices were maintained choked in order to insure no change in fuel distribution or possible coupling between combustion oscillations and fuel flow.

However, a reduced supply pressure assumedly would produce less penetration and mixing, with a possible decrease in efficiency. A fuel supply pressure of 108 inches of mercury absolute and a spray-bar system of 0.023-inch-diameter orifices delivered the same fuel flow (afterburner equivalence ratio approx. 0.54) as a pressure of only 30 inches of mercury absolute with 0.046-inch-diameter orifices. Figure 13 shows that the change in efficiency was only about 4 points and that, over the

range tested, the efficiency spread was still approximately 4 percent. Since the efficiency curves did not fall in the same order as the supply-pressure curves, it appears that the 0.033-inch-diameter orifice configuration was the optimum tested on the basis of fuel penetration, mixing, and efficiency. It can therefore be concluded that, for the particular injector configurations reported, lowering the supply pressure for a given fuel flow had only a small effect on efficiency.

Effect of fuel-bar size. - Since fuel bars provide recirculatory zones that may be important to flame stabilization, fuel bars of three different diameters were tested. The trend of combustion efficiency with equivalence ratio was similar for bars of 3/8-, 1/2-, and 5/8-inch diameter, as shown in figure 14. The efficiency level at a given equivalence ratio also was not affected to any great extent by the change in bar size. The flame stability for the larger bars was better at the lean fuel flows, as indicated by the greater operating range. As expected, increasing the bar size from 3/8- to 5/8-inch diameter resulted in a pressure-loss increase (about $2\frac{1}{2}$ points at balanced-cycle condition). The efficiency for the balanced-cycle condition was approximately 10 points higher for configuration G than for configurations E or F. This increase may be explained by the fact that the higher flow resistance of configuration G (due to higher blockage) produced limiting turbine-outlet temperature (1700° R) at a lower afterburner heat release and, hence, a lower equivalence ratio. Since the curves have the same characteristic shape, the efficiency for configuration G is higher. The high level of pressure loss ($\Delta P/P$) should not be considered a penalty for the types of configurations tested, since it results from the selection of a high afterburner velocity, chosen to provide severe combustion conditions in order to magnify any improvements resulting from modifications.

Combustion Efficiency Comparison, Configurations A and B

The data already discussed show a marked drop in efficiency in the range of equivalence ratios from 0.5 to 1.0. The peaking of the efficiency curves at lean equivalence ratios indicates stratification and extremely little penetration and mixing. For afterburner application where maximum thrust is desired, efficient burning at an afterburner equivalence ratio approaching 1.0 is required. From the preceding data, it appears that additional points of injection are required for a more homogeneous fuel-air mixture, and, in view of this, a modified ring-type fuel injector (configuration B) was constructed with orifice spacing based on the mass-flow profile. Configuration B had a hole density of 4.15 holes per square inch of burner area, whereas configuration A had a hole density of 2.12. (The configuration in ref. 4 had a hole density of 4.45.) The comparison of the two injectors investigated is shown in figure 15. The modification (configuration B) raised the combustion

[redacted]

efficiency at a given equivalence ratio 8 to 10 points and greatly improved the lean operating range. However, peak efficiency still occurred at a lean equivalence ratio, and the drop in efficiency on either side of the peak was still rapid. For example, a change in equivalence ratio of 0.1 point on either side of the peak dropped the efficiency 4 to 9 points. Configuration B, because of its greater blockage and higher heat release for a given equivalence ratio, had the expected higher pressure loss.

The conclusion can be made that the rapid decrease in efficiency from peak values shows fuel distribution to be a major problem in afterburner design for hydrogen fuel. One solution for improvement on the lean side, at least, might be to stratify the burning zone by using some combination of splitter plates and multiple-injector system rather than to attempt a further increase in the number of injection holes in a single-injector system. The possibilities of mixers, flameholders, or other turbulence-generating and flame-stabilization systems also remain to be evaluated.

Performance for Two Afterburner Lengths

A comparison of burner performance for two afterburner lengths, 27 and 39 inches, at two pressure levels is shown in figure 16. For the higher pressure condition the reduction of the burner length by 12 inches had no effect on the balanced-cycle efficiency but did reduce the peak efficiency and lean stability limits. For the lower pressure condition, the same reduction in length resulted in a 20-point drop in balanced-cycle and peak efficiency. Lean operating range at both pressure levels was improved by the additional burning length. The pressure loss was increased 1 point for the longer burner.

From these data, it can be concluded that the burner length becomes increasingly important at reduced burner pressures. Also, it appears that a burner length of over 3 feet will be required for efficient operation at these low pressures and high velocities with a burner having no flame-stabilizing device other than the fuel injectors.

Balanced-Cycle Operation

In regard to the variation in absolute performance values with equivalence ratio, only those obtained at balanced-cycle conditions are significant in afterburner work. The variation in afterburner-inlet environment with equivalence ratio for different constant-area exhaust nozzles and the balanced-cycle performance obtained therefrom are shown in figures 17 and 18 for configuration B at two pressure levels. For operation with the constant-area nozzle, both burner-inlet temperature and pressure

increased with equivalence ratio (fig. 17) as expected, because of the greater heat release associated with the higher fuel flows; the larger nozzles, of course, permit greater heat addition before limiting turbine-outlet temperature is reached. The variation in burner-inlet velocity for different nozzle sizes and equivalence ratios results from the associated effects of burner environment on the engine pumping characteristics. The absolute variation in balanced-cycle efficiency with equivalence ratio is shown in figure 17 by the heavy lines that connect the individual balanced-cycle points for each nozzle.

Balanced-cycle performance for afterburner pressures of 890 and 488 pounds per square foot absolute are summarized in figure 18. The maximum combustion efficiencies were approximately 94 and 78 percent, obtained at equivalence ratios between 0.3 and 0.4, for burner pressures of 890 and 488 pounds per square foot absolute, respectively. A serious drop-off in efficiency occurred as the equivalence ratio was increased beyond that for peak efficiency. At an equivalence ratio of 0.8, corresponding efficiencies had dropped to 77 and 68 percent. The pressure-loss increase for balanced-cycle conditions was approximately linear with increase in equivalence ratio; extrapolation indicates a dry pressure loss between 4 and 5 percent (fig. 18).

CE-2

A performance comparison of hydrogen and JP-4 fuels is shown in figure 19. The JP-4 curves are the result of cross plots and represent, at the present time, good performance for an afterburner. Although the hydrogen fuel curves (same as fig. 12) are not at balanced-cycle conditions as are the JP-4 curves, the efficiencies should be conservative compared with the values that should be attainable at balanced-cycle conditions with a variable-area nozzle.

It should be pointed out, in regard to the preceding comparison, that at more extreme afterburner conditions the margin of difference probably would be considerably greater in favor of the hydrogen fuel. Also, the performance reported herein represents early hydrogen afterburner development data, as contrasted to many years of research with JP-4 fuel.

In summing up the balanced-cycle operation of configuration B, the major conclusion is that, from the standpoint of maximum burner output (stoichiometric operation), the trend of efficiency with increase in equivalence ratio indicates a definite need for further afterburner development.

Operational Observations

Autoignition (as observed by periscope) always resulted at burner-inlet temperatures of approximately 1100° F or higher for all conditions

investigated. Similar spontaneous ignition characteristics are also reported in reference 4.

Burning took place across the entire combustor immediately upon the start of fuel flow; no coupling reaction occurred (with ignition propagating from one fuel injector to another and, finally, full burner operation) as is sometimes observed with hydrocarbon fuels. Operation with fuel injectors of the ring-type resulted in definite concentric light blue and dark blue flame rings, with the lighter rings corresponding to the location of the fuel rings. The light and dark rings indicated a lack of fuel penetration and a need either for more finely distributed points of fuel injection or for better means of mixing fuel and air uniformly. The same flame characteristics were noted for the bar-type injectors, in which case the lighter flame regions were radial in direction.

No cooling or structural problems were encountered for the fuel injectors investigated (all injector configurations had 1/32-in. walls with the exception of the trunks on the ring configurations, which were 1/16-in. wall).

Some periscopic observations, made when combustion occurred outside of the afterburner, indicated a need for a flame stabilizer. This phenomenon was noted generally at conditions of extremely low burner pressure, short burner length, and downstream injection.

The occurrence of audible screech for all configurations investigated is presented in figure 20. The data points represent steady-state operation in screech. No attempt was made to evaluate or eliminate screech; however, a tape recording using a microphone located outside the test chamber revealed a screech frequency of approximately 1000 cycles per second. Screech was never encountered at equivalence ratios below 0.4, and no structural damage due to screech was noted under the conditions investigated. However, screech possibly might have been eliminated by some means employed in reference 13.

SUMMARY OF RESULTS

The results presented herein represent an evaluation of the use of hydrogen fuel in a full-scale afterburner and are summarized as follows:

The combustion efficiency was not significantly affected by the direction of fuel injection. However, based on stability characteristics, the injection upstream, 45° downstream, or downstream appeared most desirable. Variation in fuel supply pressure (and penetration) affected the combustion efficiency only slightly. In the range covered, the efficiency level was not significantly affected by the diameter of the radial fuel-injector bars. The efficiency of the concentric-ring-type fuel

injector was improved on the lean side by increasing the number of injection orifices, whereas the rich side was not appreciably changed.

A method for obtaining adequate mixing of the fuel and air in addition to uniform fuel injection is necessary in the design of an efficient hydrogen fuel-injection system.

Afterburner length becomes increasingly important for burner-inlet pressures of about 500 pounds per square foot absolute and lower.

The maximum combustion efficiencies at balanced-cycle conditions for the modified ring-type fuel injector in a 39-inch burner were 94 and 78 percent for burner pressures of 890 and 488 pounds per square foot absolute, respectively.

Throughout the text, emphasis was placed on the severe drop in afterburner efficiency at high equivalence ratios beyond those for peak efficiency. This is a serious shortcoming, since an afterburner is normally used most effectively at high equivalence ratios. The decreasing trend in efficiency with increasing equivalence ratio is believed to be associated with severe local variations in fuel-air ratio. Possible causes of these variations could be the separated flow regions on the inner body, wakes from struts, or oscillations present with screech. Since all configurations screeched at high equivalence ratios at all burner pressure levels investigated, the next logical step would be to eliminate screech.

CE-2 back

Autoignition always resulted at an afterburner-inlet temperature of approximately 1100° F, or higher over the test range investigated. Some audible screech of about 1000 cycles per second was noted at equivalence ratios greater than 0.4.

Lewis Flight Propulsion Laboratory
National Advisory Committee for Aeronautics
Cleveland, Ohio, August 13, 1957

APPENDIX A

SYMBOLS

The following symbols are used in this report:

A	cross-sectional area, sq ft
C_T	expansion coefficient (assumed = 1.0, water-cooled throat)
C_d	discharge coefficient
f/a	fuel-air ratio
g	acceleration due to gravity, 32.2 ft/sec^2
m	mass flow, lb-sec^2/ft
P	total pressure, lb/sq ft
R	gas constant, 1544/molecular weight, ft-lb/(lb)($^\circ$R)
T	total temperature, $^\circ$R
w	weight flow, lb/sec
γ	ratio of specific heats
η	combustion efficiency
φ	equivalence ratio, percentage of stoichiometric fuel-air ratio

Subscripts:

a	air
ab	afterburner
e	engine
f	fuel
g	gas
id	ideal
mv	midframe vent

[redacted]

N	nozzle throat
st	stoichiometric
t	total
1	engine inlet
5	diffuser inlet
9	exhaust-nozzle inlet

[redacted]

APPENDIX B

METHODS OF CALCULATION

The engine-inlet and minor airflows are calculated by means of the one-dimensional flow parameters given in reference 14. The equation is:

$$w_{a,1} = \left(\frac{m\sqrt{gRT_1}}{P_1 A_1}\right) \frac{P_1 A_1}{\sqrt{R/g}\sqrt{T_1}}$$

where

$\frac{m\sqrt{gRT}}{PA}$ is the reciprocal of the total-pressure parameter and is a function of the static- to total-pressure ratio and of the ratio of specific heats ($\gamma = 1.4$), and where A is the calibrated area of the measuring station.

The diffuser-inlet airflow is defined as the engine-inlet airflow minus the bleed flow:

$$w_{a,5} = w_{a,1} - w_{a,mv}$$

The exhaust-gas temperature is calculated (choked exhaust nozzle) by using the exhaust-nozzle-inlet total pressure and the continuity equation and results in the following equation:

$$T_9 = \left(\frac{P_9 A_N C_T C_d}{w_{g,9}\sqrt{R/g}}\right)^2 \frac{\gamma_9}{\left(\frac{\gamma_9 + 1}{2}\right)^{\frac{\gamma_9+1}{\gamma_9-1}}}$$

where

$w_{g,9} = w_{a,5}\left[1 + (f/a)_t\right]$ and $C_d = 0.973$, as obtained from exhaust-nozzle data for nonburning conditions.

The afterburner combustion efficiency is defined as the ideal afterburner equivalence ratio divided by the measured afterburner equivalence ratio and may be written

$$\eta_{ab} = \frac{\varphi_{ab,id}}{\varphi_{ab}}$$

[redacted]

where

$\varphi_{ab,id} = \frac{\varphi_{t,id} - \varphi_{e,id}}{1 - \varphi_{e,id}}$; $\varphi_{t,id}$ is obtained from the temperature rise across engine-afterburner combination for blends of JP-4 and hydrogen fuel, similar to method presented in reference 15; $\varphi_{e,id}$ comes from the temperature rise across the engine, as in reference 15, and

$$\varphi_{ab} = \frac{\varphi_t - \varphi_{e,id}}{1 - \varphi_{e,id}}$$

$$\varphi_t = \varphi_e + \varphi_{ab}$$

$$= \frac{w_{f,e}/w_{a,5}}{(f/a)_{st,e}} + \frac{w_{f,ab}/w_{a,5}}{(f/a)_{st,ab}}$$

Fuel characteristics used in the calculations are:

Lower heating value (hydrogen), 51,571 Btu/lb (purity, 98 percent)

Lower heating value (JP-4), 18,670 Btu/lb

$(f/a)_{st(Hydrogen)} = 0.02916$

$(f/a)_{st(JP-4)} = 0.0672$

REFERENCES

1. Jonash, Edmund R., Smith, Arthur L., and Hlavin, Vincent F.: Low Pressure Performance of a Tubular Combustor with Gaseous Hydrogen. NACA RM E54L30a, 1955.

2. Silverstein, Abe, and Hall, Eldon W.: Liquid Hydrogen as a Jet Fuel for High-Altitude Aircraft. NACA RM E55C28a, 1955.

3. Dangle, E. E., and Kerslake, William R.: Experimental Evaluation of Gaseous Hydrogen Fuel in a 16-Inch-Diameter Ram-Jet Engine. NACA RM E55J18, 1955.

4. Kerslake, W. R., and Dangle, E. E.: Tests with Hydrogen Fuel in a Simulated Afterburner. NACA RM E56D13a, 1956.

[redacted]

5. Krull, H. George, and Burley, Richard R.: Effect of Burner Design Variables on Performance of 16-Inch-Diameter Ram-Jet Combustor Using Gaseous-Hydrogen Fuel. NACA RM E56J08, 1956.

6. Sivo, Joseph N., and Fenn, David B.: Performance of a Short Combustor at High Altitudes Using Hydrogen Fuel. NACA RM E56D24, 1956.

7. Friedman, Robert, Norgren, Carl T., and Jones, Robert E.: Performance of a Short Turbojet Combustor with Hydrogen Fuel in a Quarter-Annulus Duct and Comparison with Performance in a Full-Scale Engine. NACA RM E56D16, 1956.

8. Fleming, W. A., Kaufman, H. R., Harp, J. L. Jr., and Chelko, L. J.: Turbojet Performance and Operation at High Altitudes with Hydrogen and JP-4 Fuels. NACA RM E56E14, 1956.

9. Corrington, Lester C., Thornbury, Kenneth L., and Hennings, Glenn: Some Design and Operational Considerations of a Liquid-Hydrogen Fuel and Heat-Sink System for Turbojet-Engine Tests. NACA RM E56J18a, 1956.

10. Coss, Bert A., Daykin, D. R., Jaffe, Leonard, and Sharp, Elmer M.: A Digital Automatic Multiple Pressure Recorder. NACA TN 2880, 1953.

11. Glawe, George E., Simmons, Frederick S., and Stickney, Truman M.: Radiation and Recovery Corrections and Time Constants of Several Chromel-Alumel Thermocouple Probes in High-Temperature, High-Velocity Gas Streams. NACA TN 3766, 1956.

12. Prince, William R., Velie, Wallace W., and Braithwaite, Willis M.: Full-Scale Evaluation of Some Flameholder Design Concepts for High-Inlet-Velocity Afterburners. NACA RM E56D10, 1956.

13. Harp, James L., Jr., Velie, Wallace W., and Bryant, Lively: Investigation of Combustion Screech and a Method of Its Control. NACA RM E53L24b, 1954.

14. Turner, L. Richard, Addie, Albert N., and Zimmerman, Richard H.: Charts for the Analysis of One-Dimensional Steady Compressible Flow. NACA TN 1419, 1948.

15. Huntley, S. C.: Ideal Temperature Rise Due to Constant-Pressure Combustion of a JP-4 Fuel. NACA RM E55G27a, 1955.

[redacted]

TABLE I. - FUEL-INJECTOR CONFIGURATIONS[a]

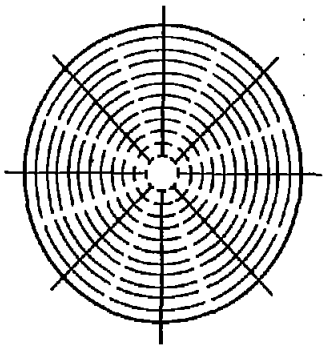

Ring

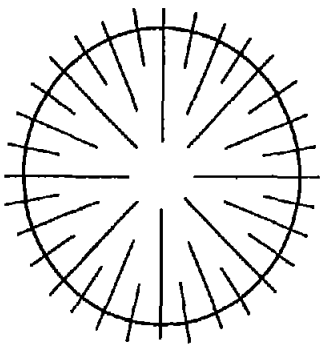

Bar

Configuration	Injector	Number of injectors	Injector diameter, in.	Orifice diameter, in.	Total number of orifices	Projected blockage, percent full-burner area	Configuration ratio shown in figure	Orifice distribution base	Remarks
A	Concentric rings	15	[b]1/4	0.033	[c]1440	25	5,8	Equally spaced	90 Percent radial with 10 percent axial upstream injection, 8 fuel sectors
B	↓	27	[d]5/32	.026	[e]2808	37	7,8	Mass-flow profile	100 Percent axial upstream injection, 8 fuel sectors
C	Radial bars	60	5/8	.023	1440	25	9,10	Area weighted	15 - 8.7-Inch and 30 - 4.7-inch bars located 1 inch downstream of 15 - 12.7-inch bars
D		60	5/8	.033	1440	25	9,10		Used in fuel-injection-direction investigation
E		60	3/8	.046	1440	25	9,10		
F		60	1/2	.046	1440	33	9,10		
G	↓	60	5/8	.045	1440	42	9,10	↓	

[a]Configurations grouped as follows:
A and B, for effect of number of orifices
C, D, and E, for effect of orifice diameter
E, F, and G, for effect of fuel-bar diameter

[b]See fig. 5.

[c]Hole density, 2.12 holes/sq in. of burner area.

[d]See fig. 7.

[e]Hole density, 4.15 holes/sq in. of burner area.

TABLE II. - RANGE OF AFTERBURNER OPERATING VARIABLES

Fuel-injector configuration	Burner configuration	Burner length, in.	Exhaust-nozzle area, percent of full-burner area	Engine-inlet pressure, P_2, lb/sq ft abs	Burner-inlet pressure, P_5, lb/sq ft abs
A	A (liner)	69	86	270	375-515
		69	86	322	476-608
		69	86	425	678-848
	B (no liner)	39	80	270	427-491
	B (no liner)	39	80	480	794-902
	A (liner)	27	70	219	371-412
				273	422-519
				322	477-646
				372	529-715
				452	624-908
B	B (no liner)	27	80	274	420-511
		27		480	708-892
		39		272	365-496
				480	665-890
			70	275	416-512
			70	481	716-927
			62	277	408-516
			62	483	675-933
C			70	275	435-505
D			70	273	404-515
D			70	479	752-950
E			80	275	425-508
			70	274	431-511
			70	479	751-897
F			80	275	385-503
F			80	483	705-927
G			86	275	389-504
			86	483	663-908
			80	275	333-502
			80	484	695-940

[redacted]

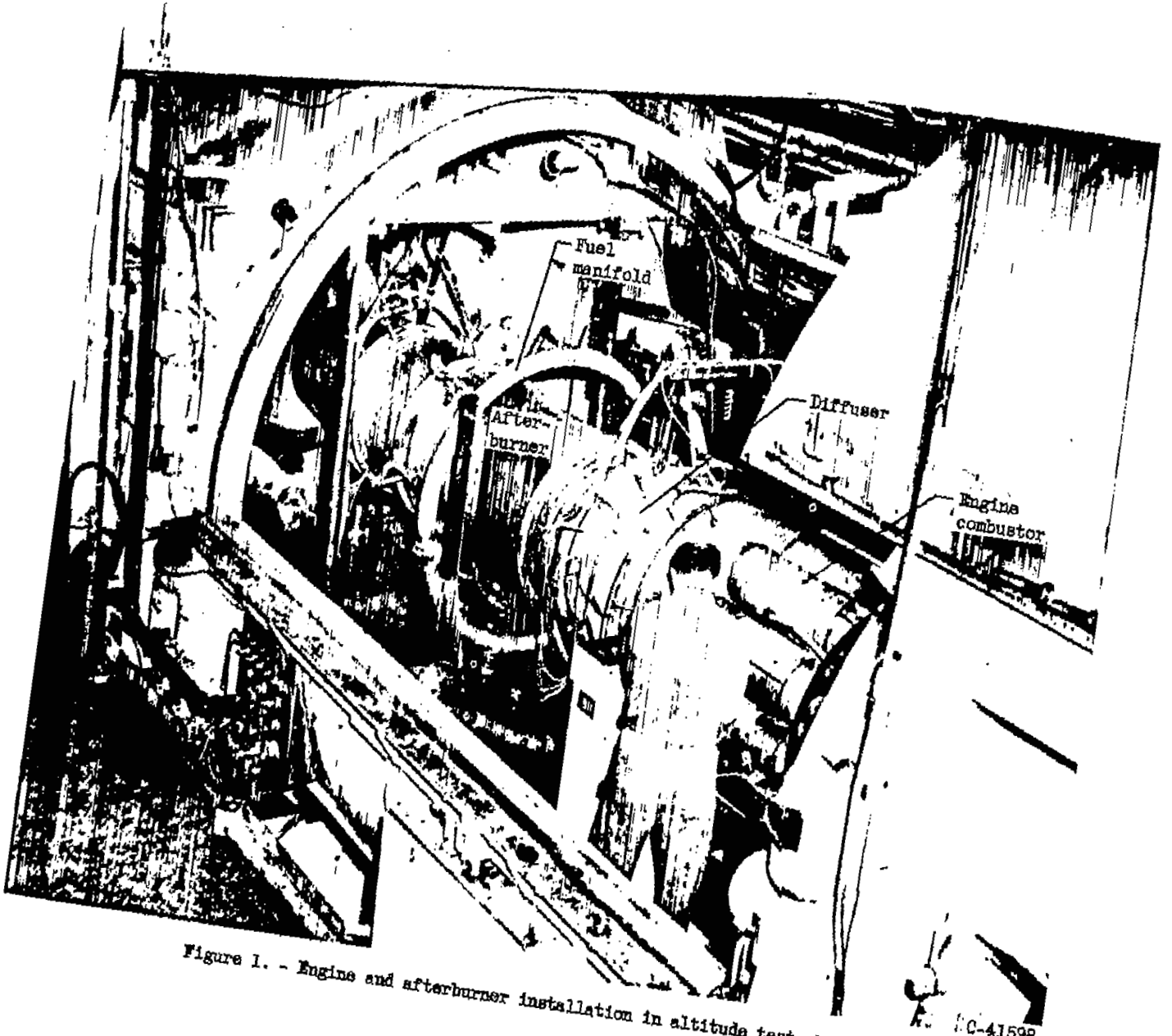

Figure 1. - Engine and afterburner installation in altitude test chamber.

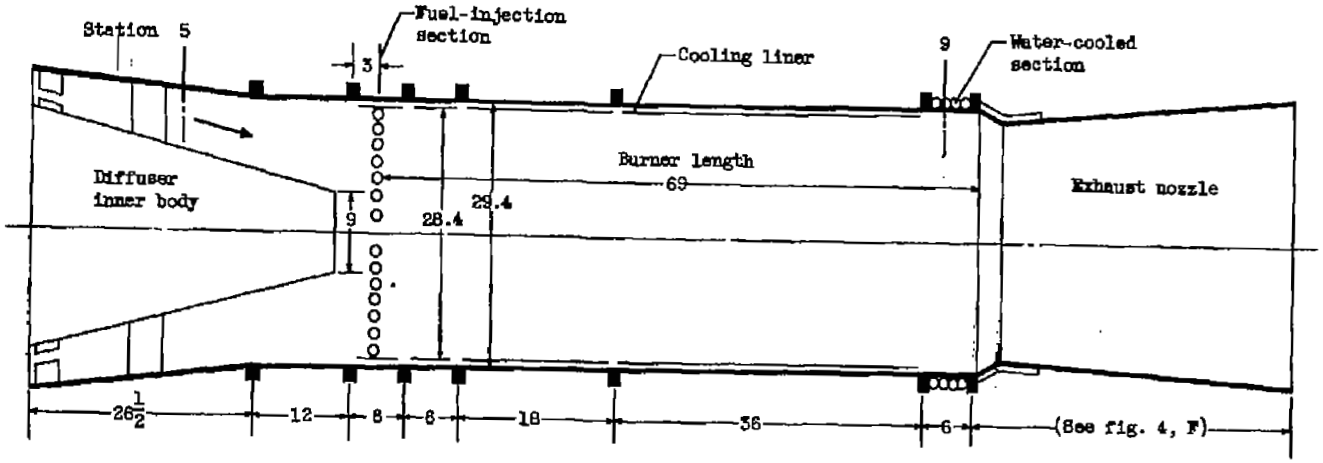

Station	Total-pressure tubes	Wall static-pressure orifices	Thermocouples
5	12 plus 1 integrating	2	16
9	13 plus 1 integrating	2	0

(a) Burner A (with liner).

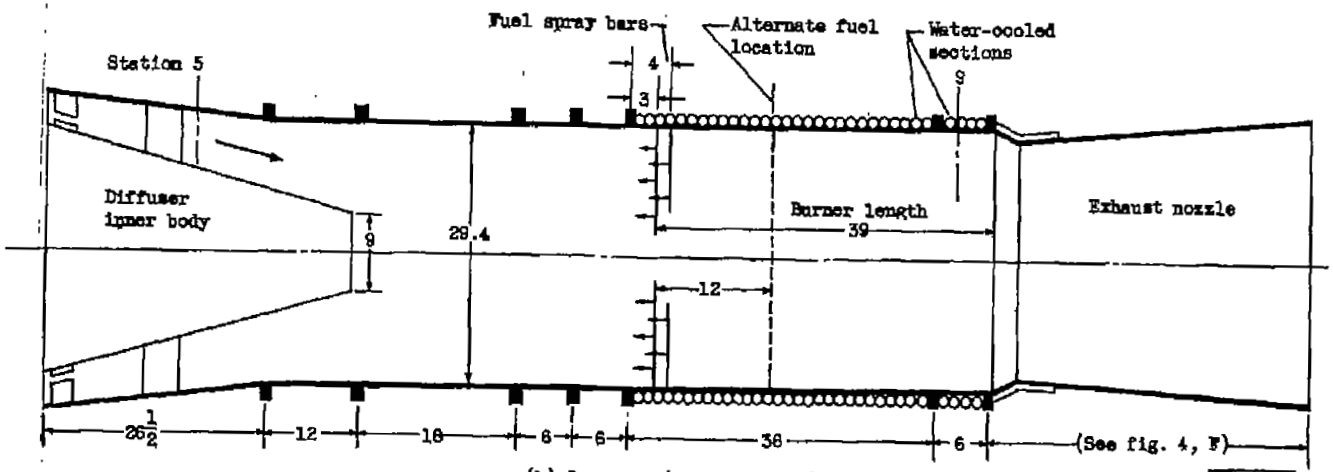

(b) Burner B (without liner).

CD-5801

Figure 2. - Details of afterburners showing location of instrumentation. (All dimensions in inches.)

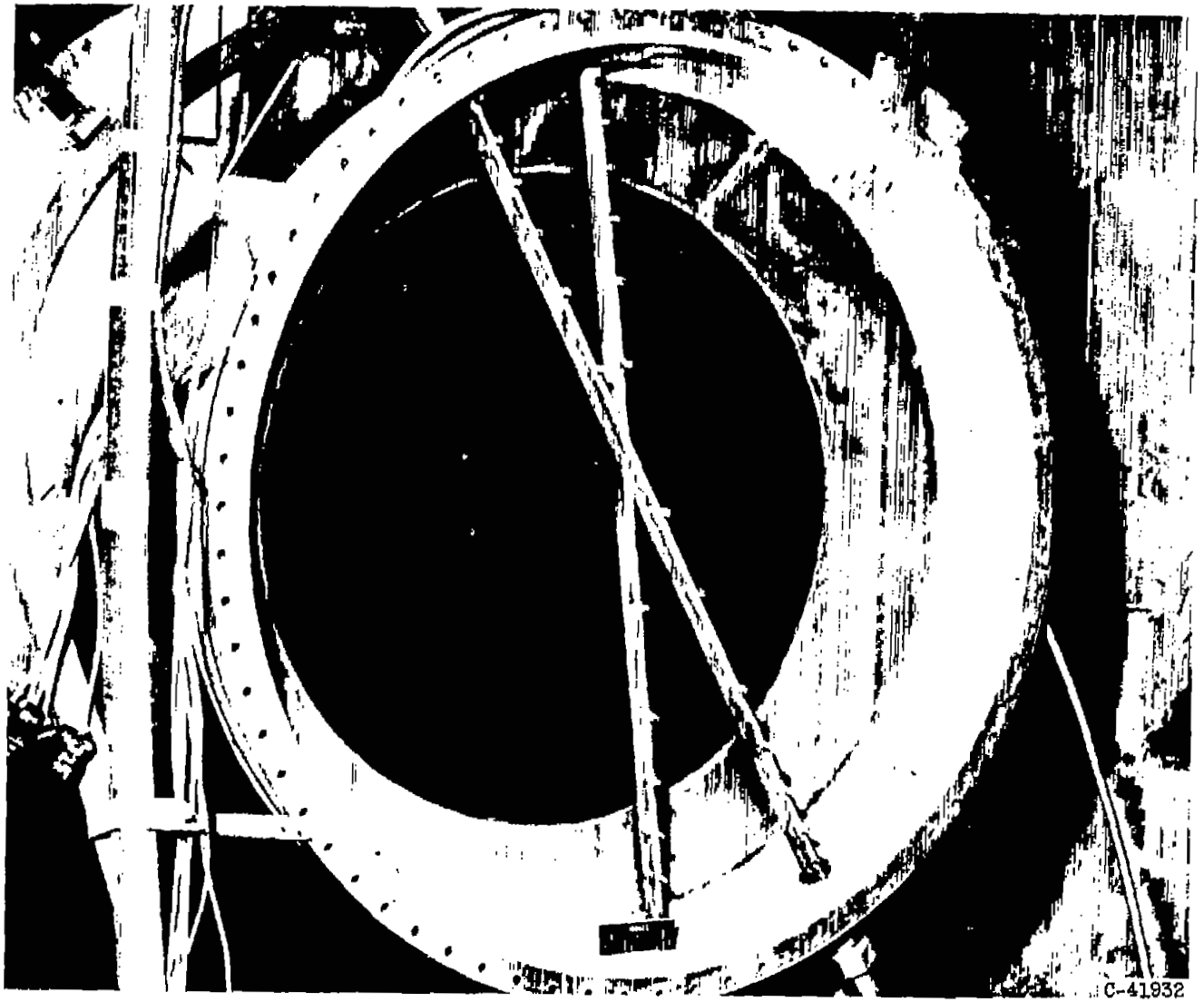

Figure 3. - Photograph showing water-cooled total-pressure rakes installed at station 9.

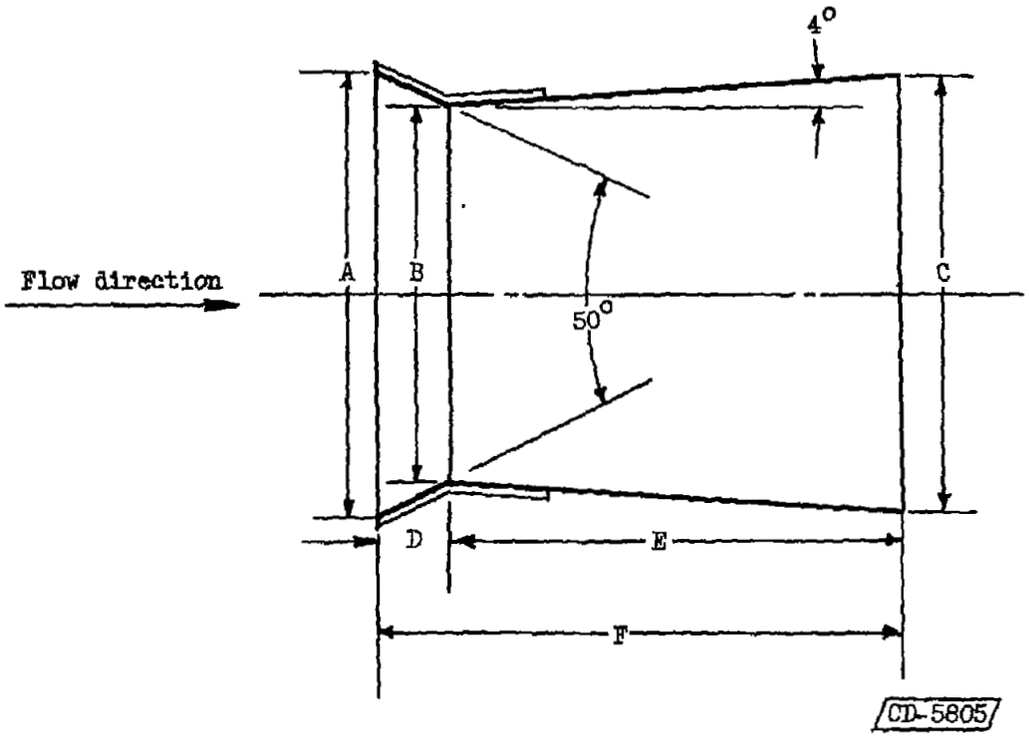

Area nozzle throat / Area full-burner, percent	Throat area, sq ft	Nozzle diameter			D, in.	E, in.	F, in.
		Inlet, A, in.	Throat, B, in.	Exit, C, in.			
86	4.0635	29.4	27.295	32.180	2.257	34.928	37.185
80	3.8013	29.4	26.400	31.125	3.217	33.784	37.001
70	3.2978	29.4	24.590	28.990	5.158	31.460	36.618
62	2.9248	29.4	23.157	27.302	6.694	29.637	36.331

(Note: For all nozzles; area exit ÷ area throat = 1.39.)

Figure 4. - Convergent-divergent exhaust nozzles.

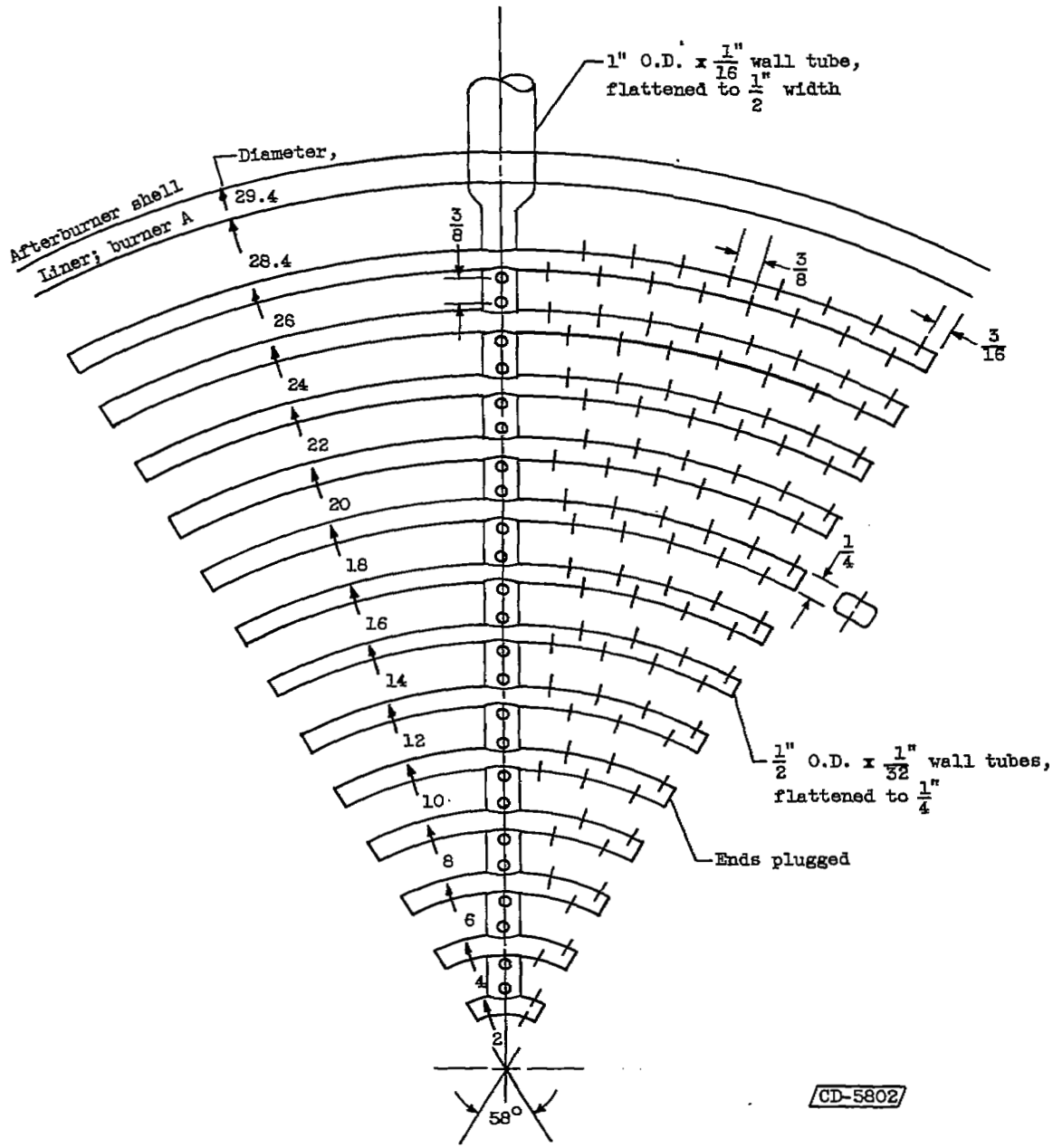

Figure 5. - Fuel-injector sector, configuration A; 6 sectors required. Injection, 90-percent radial and 10-percent axial; material, Inconel; all holes, 0.033-inch diameter; total number of holes per sector, 240 (216 in rings and 24 in trunk). (All dimension in inches.)

[redacted]

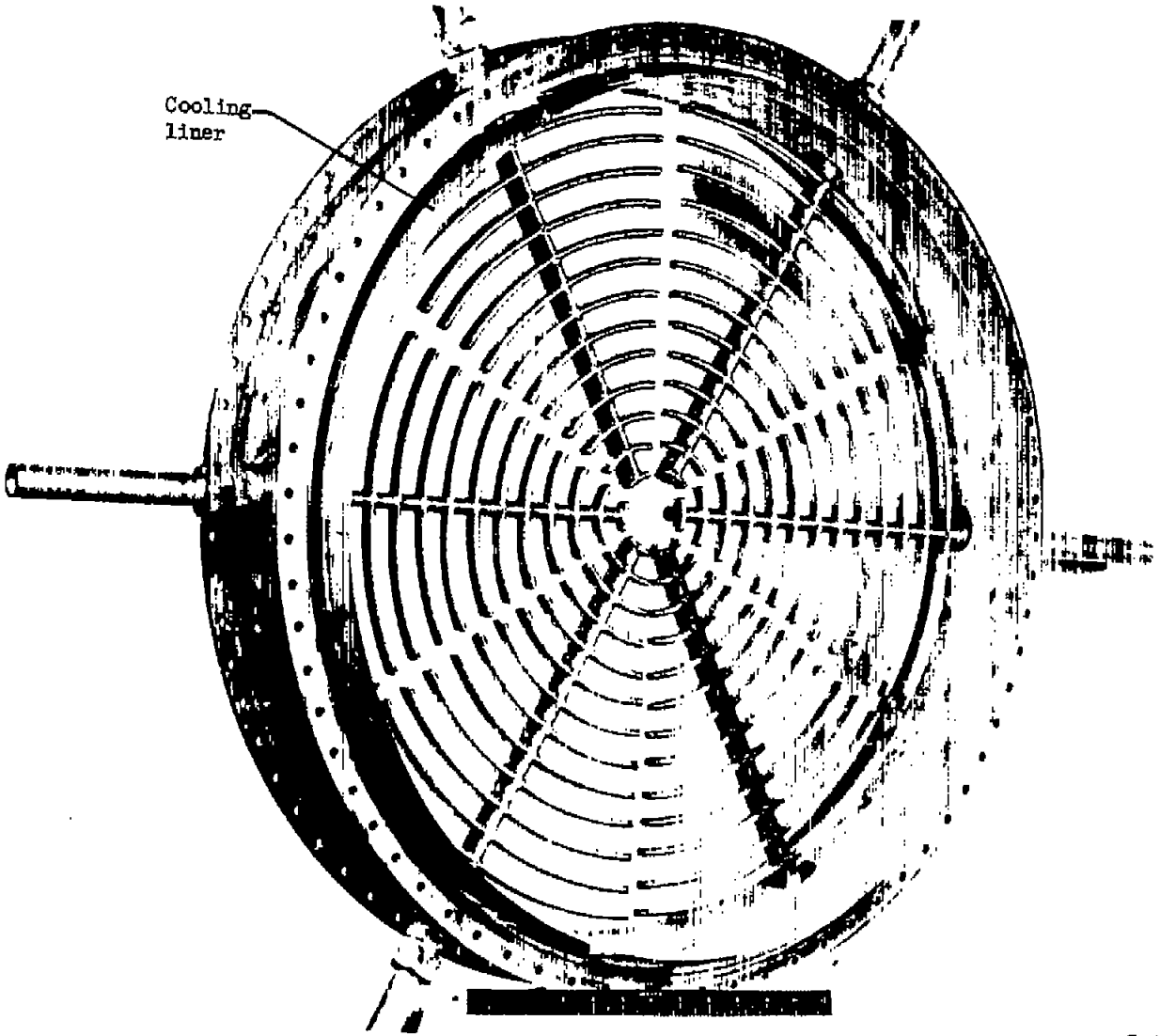

C-41486

Figure 6. - Fuel injector, configuration A.

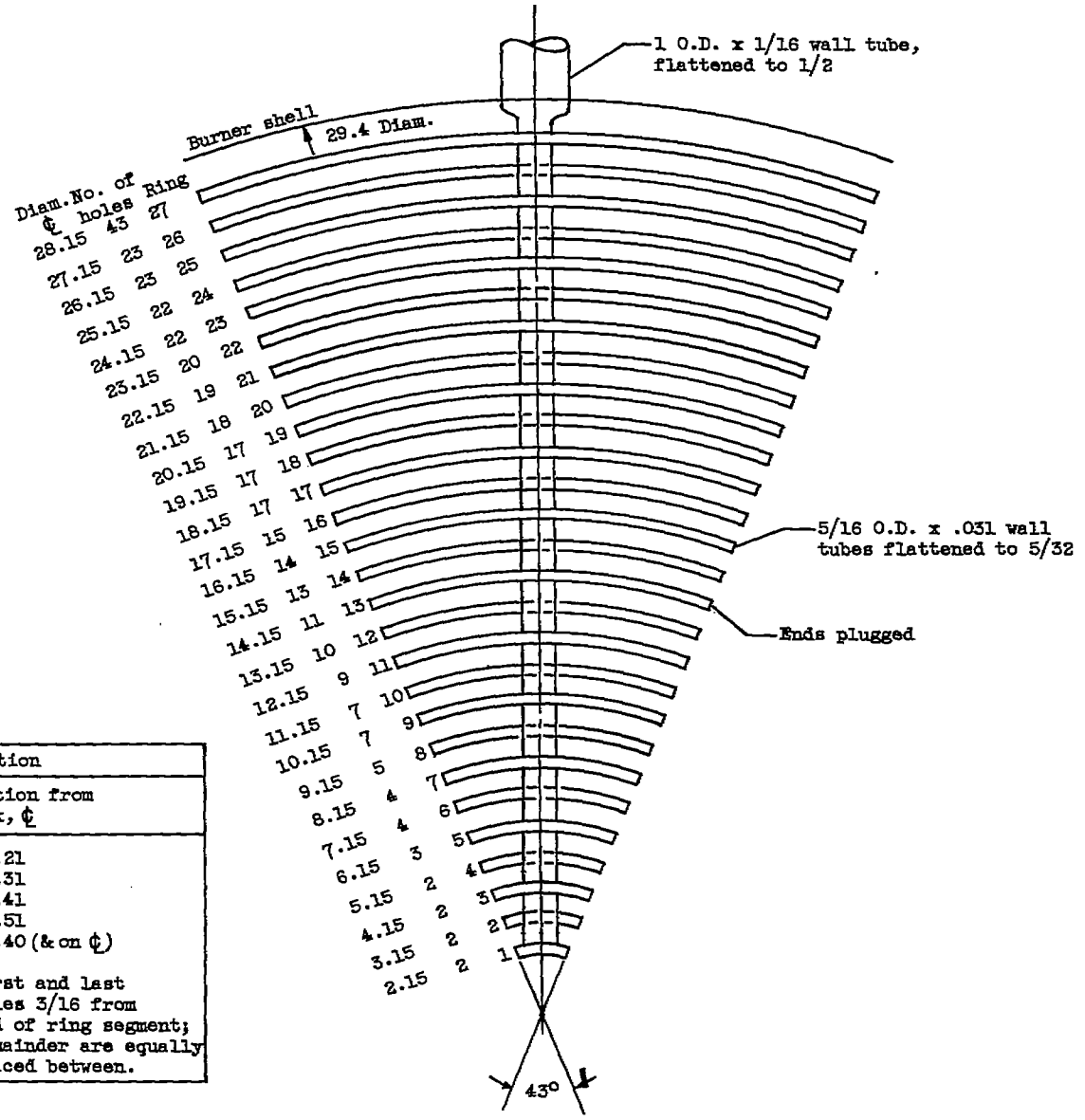

Hole location	
Ring	Location from trunk, ℄
1	±0.21
2	± .31
3	± .41
4	± .51
5	± .40 (& on ℄)
6-27	First and last holes 3/16 from end of ring segment; remainder are equally spaced between.

Figure 7. - Fuel-injector sector, configuration B; 8 sectors required. Material, Inconel; all holes, 0.026-inch diameter; all holes drilled for 100-percent axial injection. Total number of holes, 351. (All dimensions in inches.)

CH-4

[redacted]

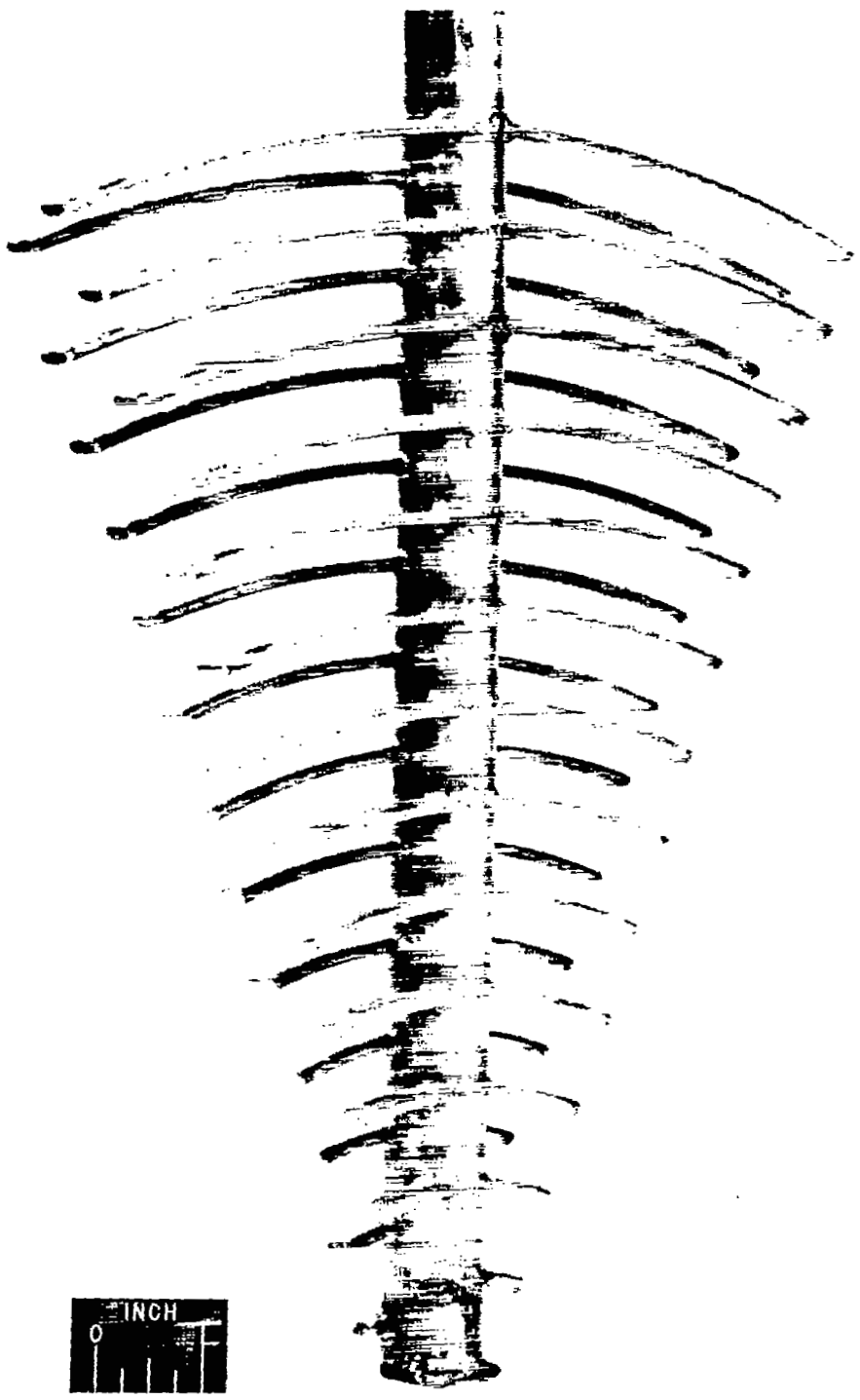

C-42184

Figure 8. - Fuel-injector sector, configuration B.

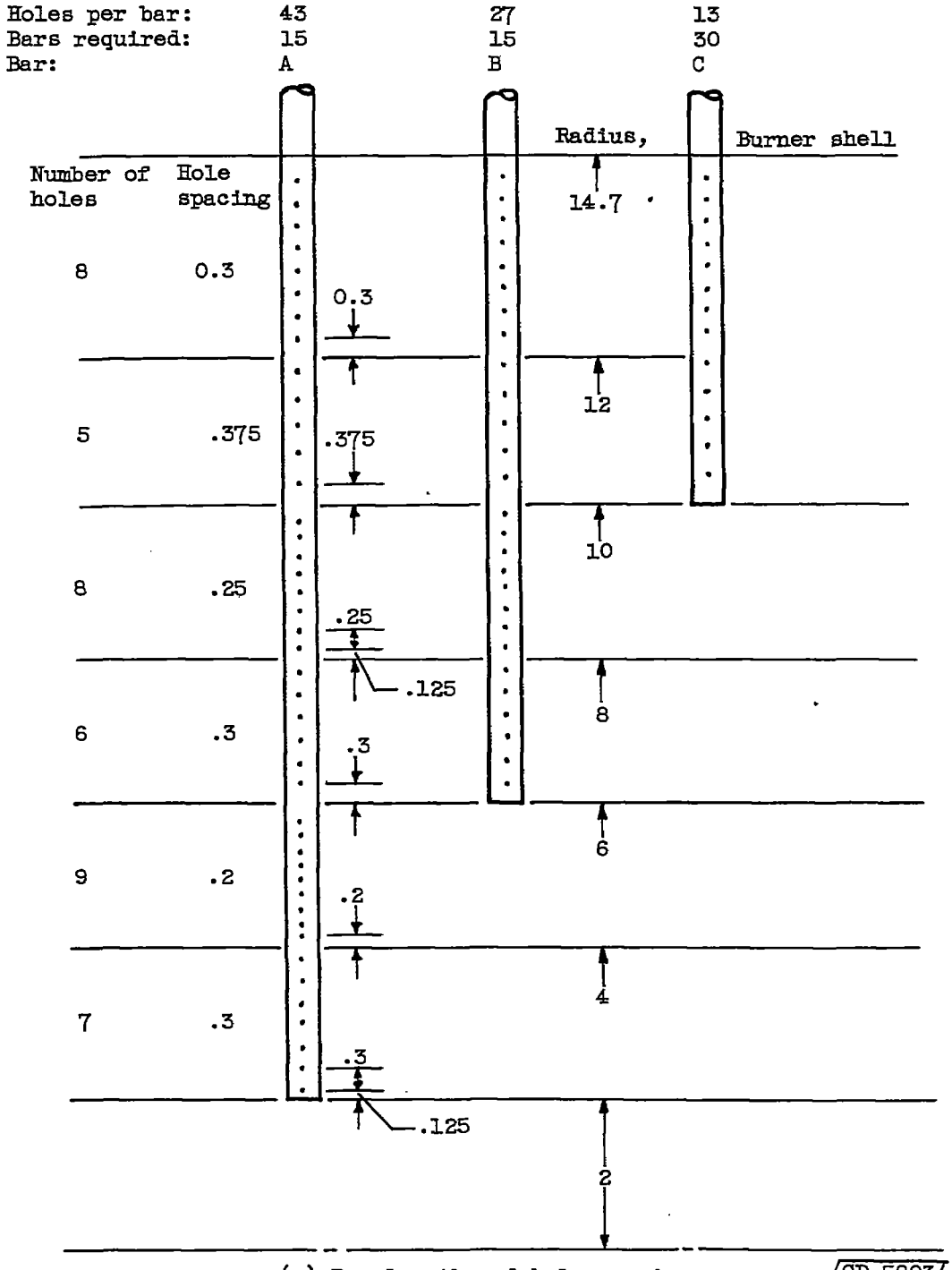

(a) Bar length and hole spacing. CD-5803

Figure 9. - Radial-bar-type fuel injectors. Configuration, C to G; material, Inconel; all bars, 1/32-inch wall diameter. (All dimensions in inches.)

CE-4 back

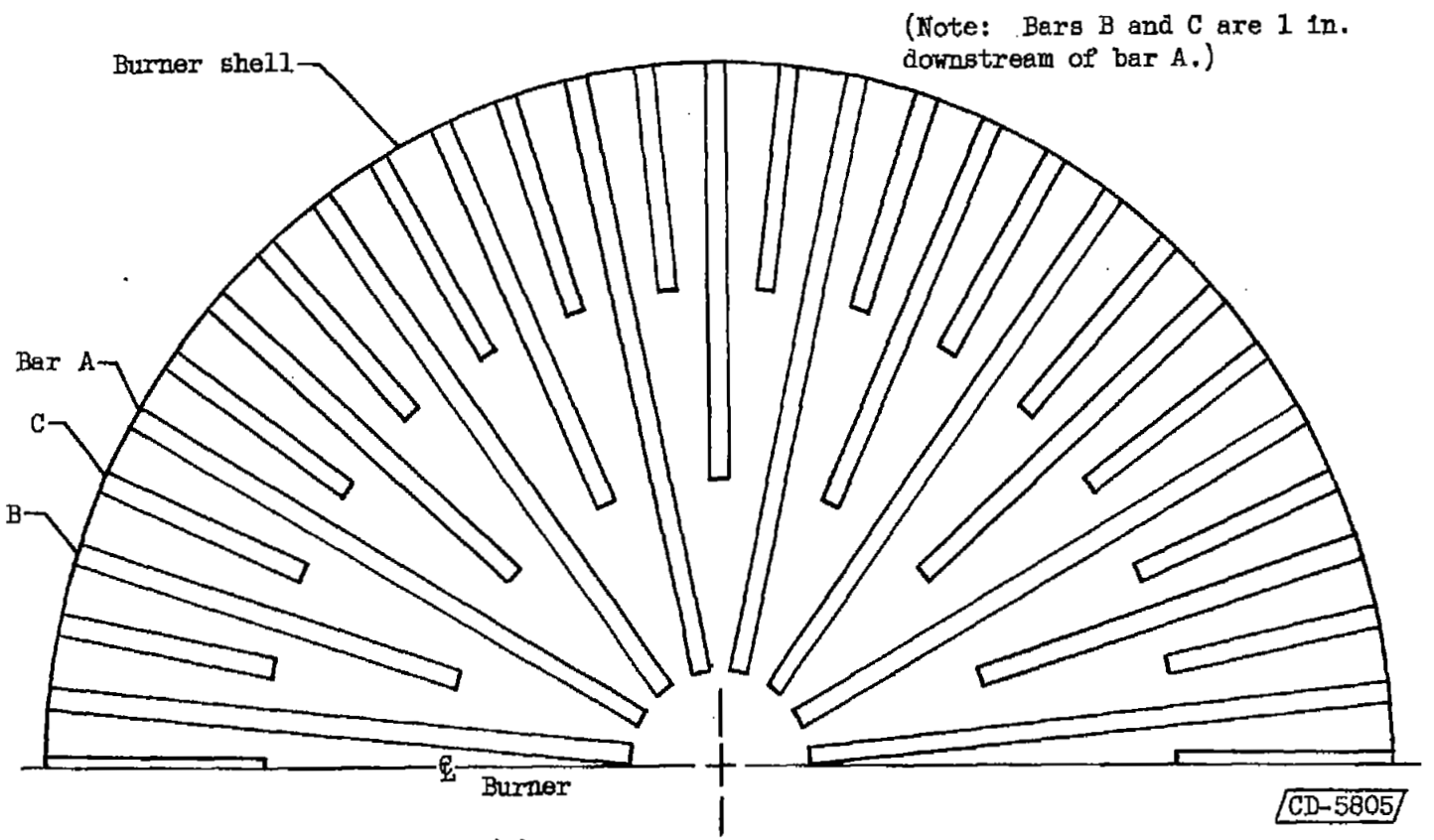

(b) Installation of radial bars.

Figure 9. - Concluded. Radial-bar-type fuel injectors. Configuration, C to G; material, Inconel; all bars, 1/32-inch wall diameter. (All dimensions in inches.)

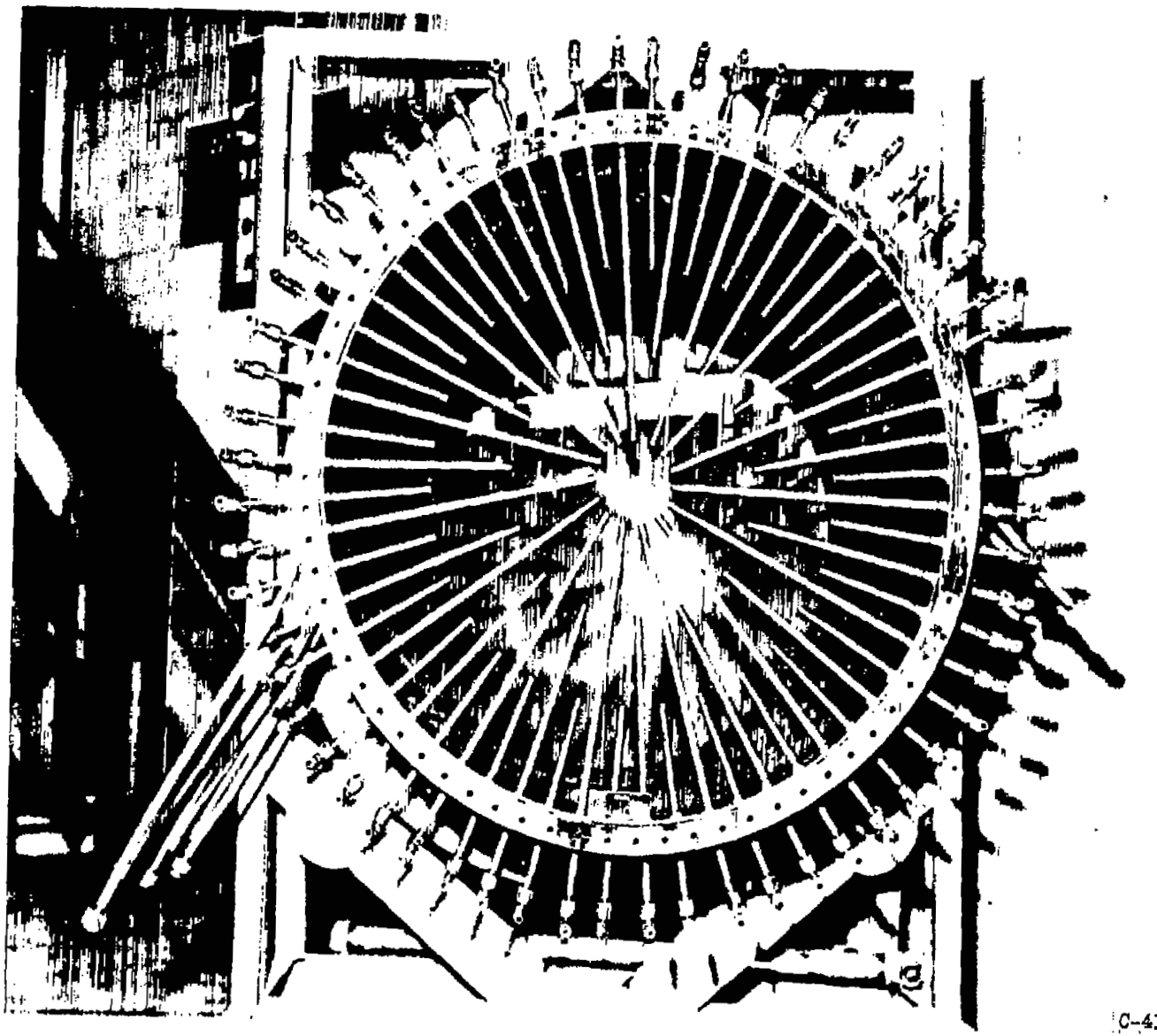

C-41933

Figure 10. - Radial-bar-type fuel injectors, configuration C.

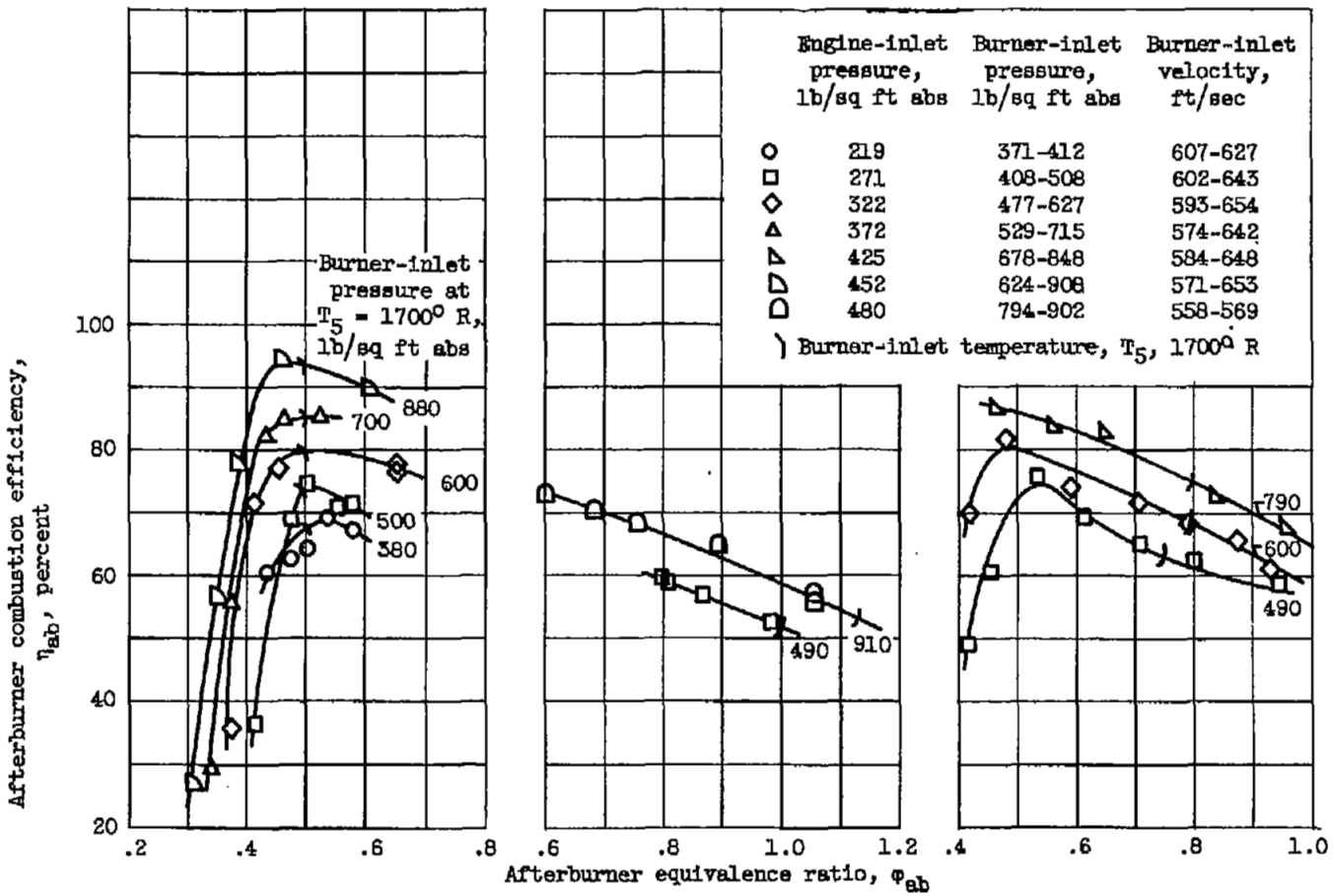

(a) Burner configuration A (fig. 2(a)); burner length, 27 inches; exhaust-nozzle area, 70 percent of full-burner area.

(b) Burner configuration B (fig. 2(b)); burner length, 39 inches; exhaust-nozzle area, 80 percent of full-burner area.

(c) Burner configuration A (fig. 2(a)); burner length, 69 inches; exhaust-nozzle area, 86 percent of full-burner area.

Figure 11. - General exploratory combustion efficiencies for configuration A.

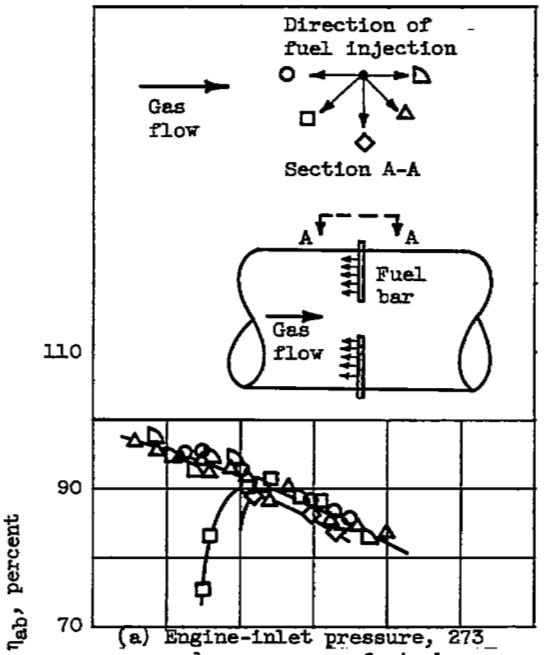

(a) Engine-inlet pressure, 273 pounds per square foot absolute; burner-inlet pressure, 404-515 pounds per square foot absolute; burner-inlet velocity, 598-633 feet per second.

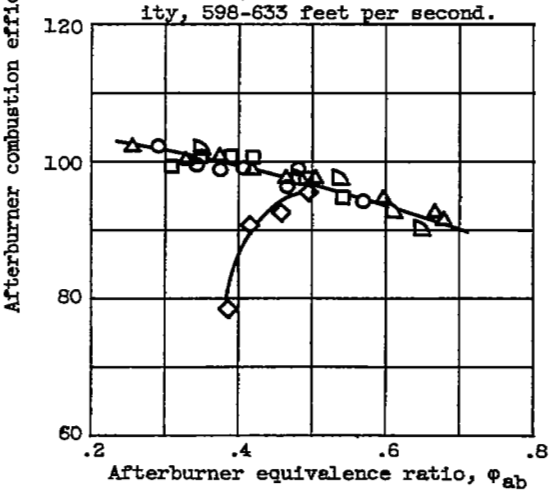

(b) Engine-inlet pressure, 479 pounds per square foot absolute; burner-inlet pressure, 752-950 pounds per square foot absolute; burner-inlet velocity, 562-571 feet per second.

Figure 12. - Effect of direction of fuel injection, configuration D. Exhaust-nozzle area, 70 percent of full-burner area; burner length, 39 inches.

[redacted]

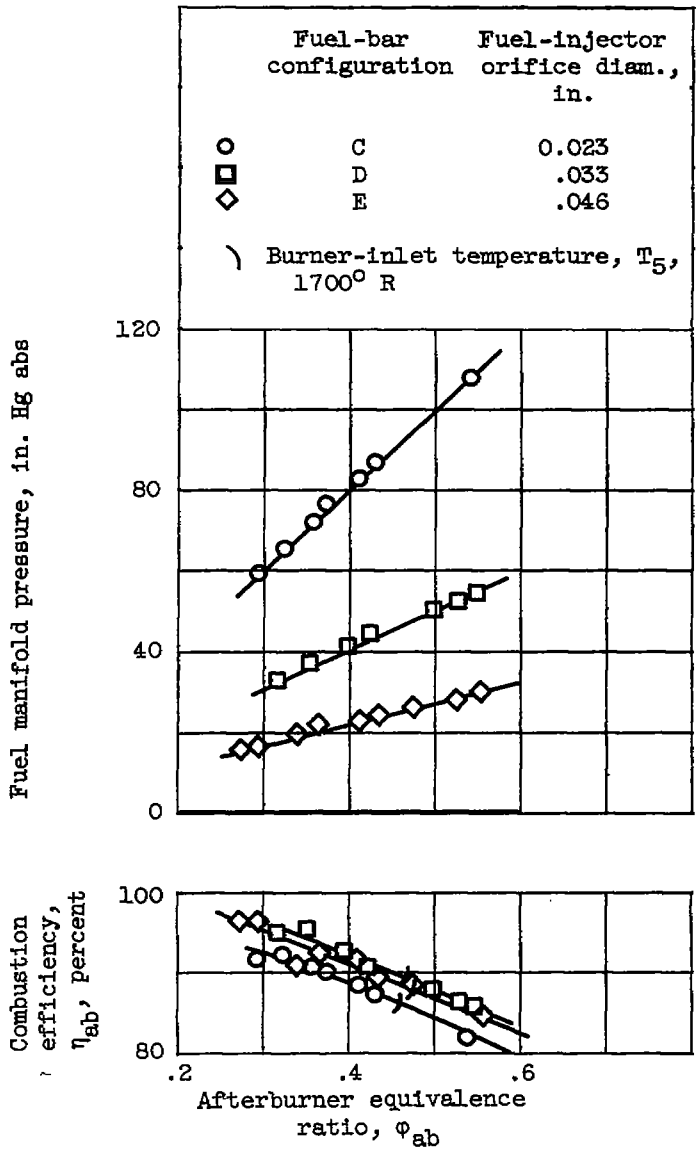

Figure 13. - Effect of fuel-injector orifice diameter (upstream injection). Exhaust-nozzle area, 70 percent of full-burner area; burner length, 39 inches; engine-inlet pressure, 274 pounds per square foot absolute; burner-inlet pressure, 423 to 510 pounds per square foot absolute; burner-inlet velocity, 585 to 617 feet per second.

[redacted]

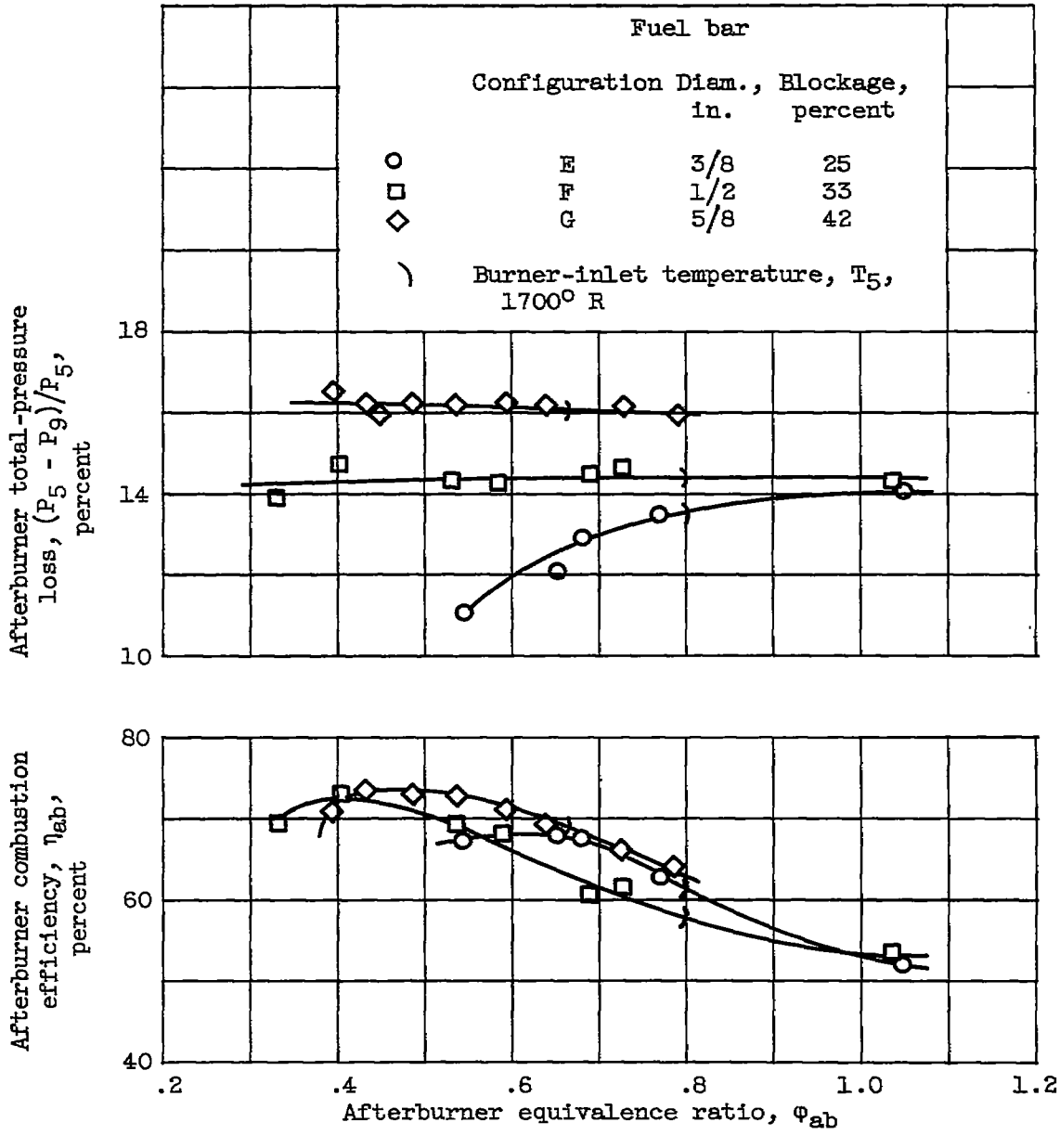

Figure 14. - Effect of fuel-bar size (upstream injection). Exhaust-nozzle area, 80 percent of full-burner area; burner length, 39 inches; engine-inlet pressure, 275 pounds per square foot absolute; burner-inlet pressure, 381 to 504 pounds per square foot absolute; burner-inlet velocity, 608 to 647 feet per second.

CE-5

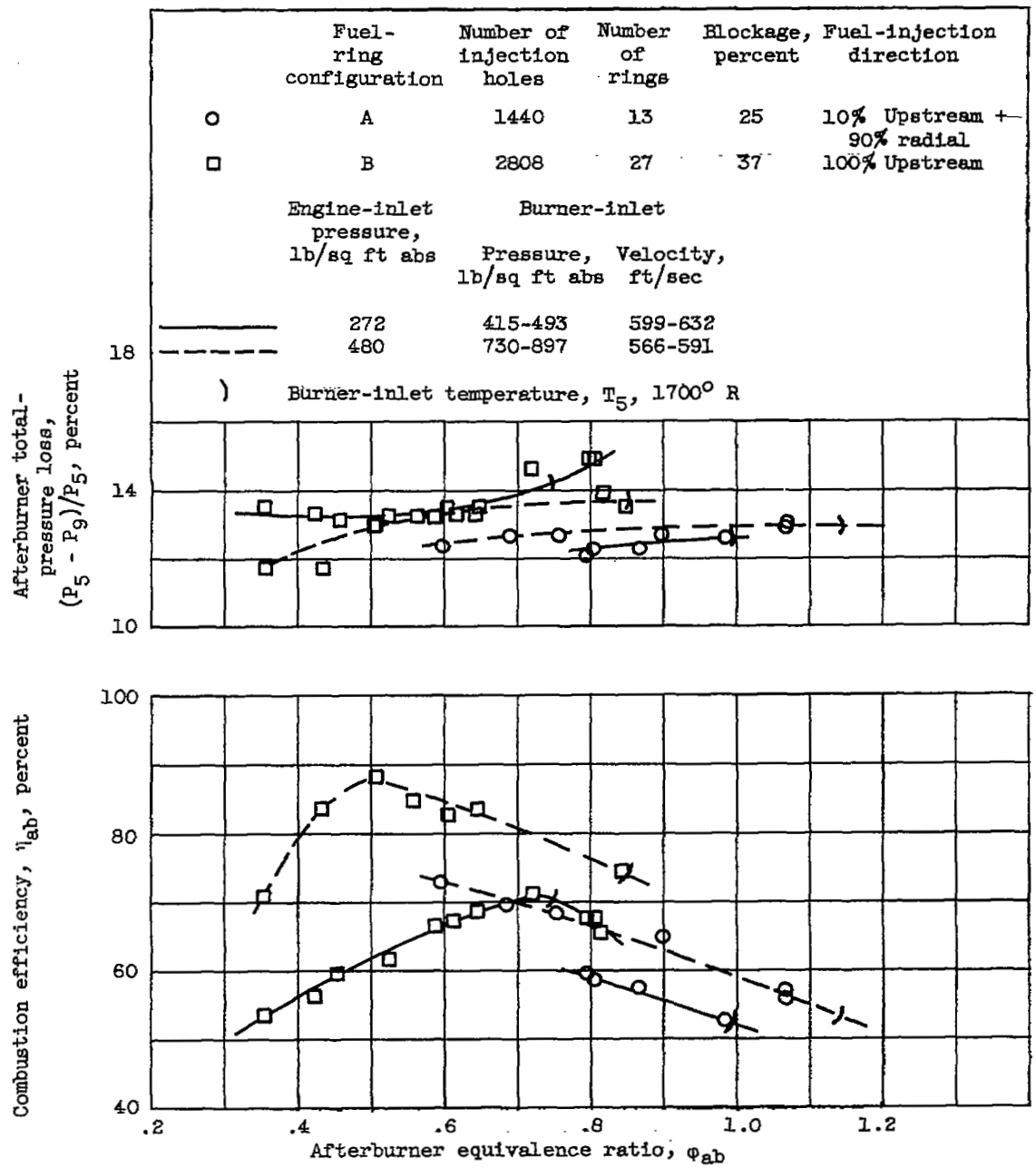

Figure 15. - Performance comparison of two concentric-ring-type fuel injectors. Exhaust-nozzle area, 80 percent of full-burner area; burner length, 39 inches.

CE-5 back

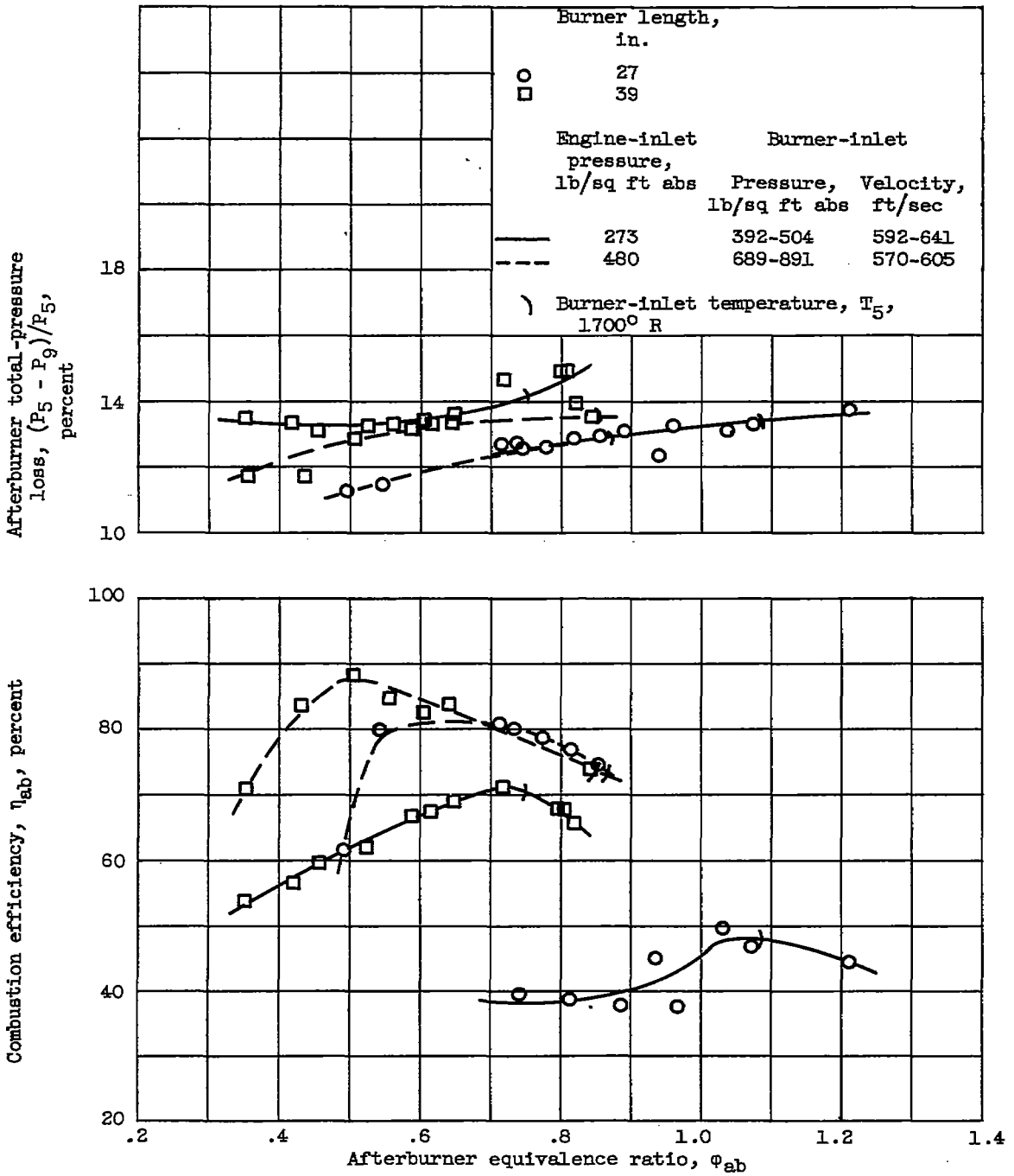

Figure 16. - Afterburner performance for two burner lengths, fuel-ring configuration B. Exhaust-nozzle area, 80 percent of full-burner area.

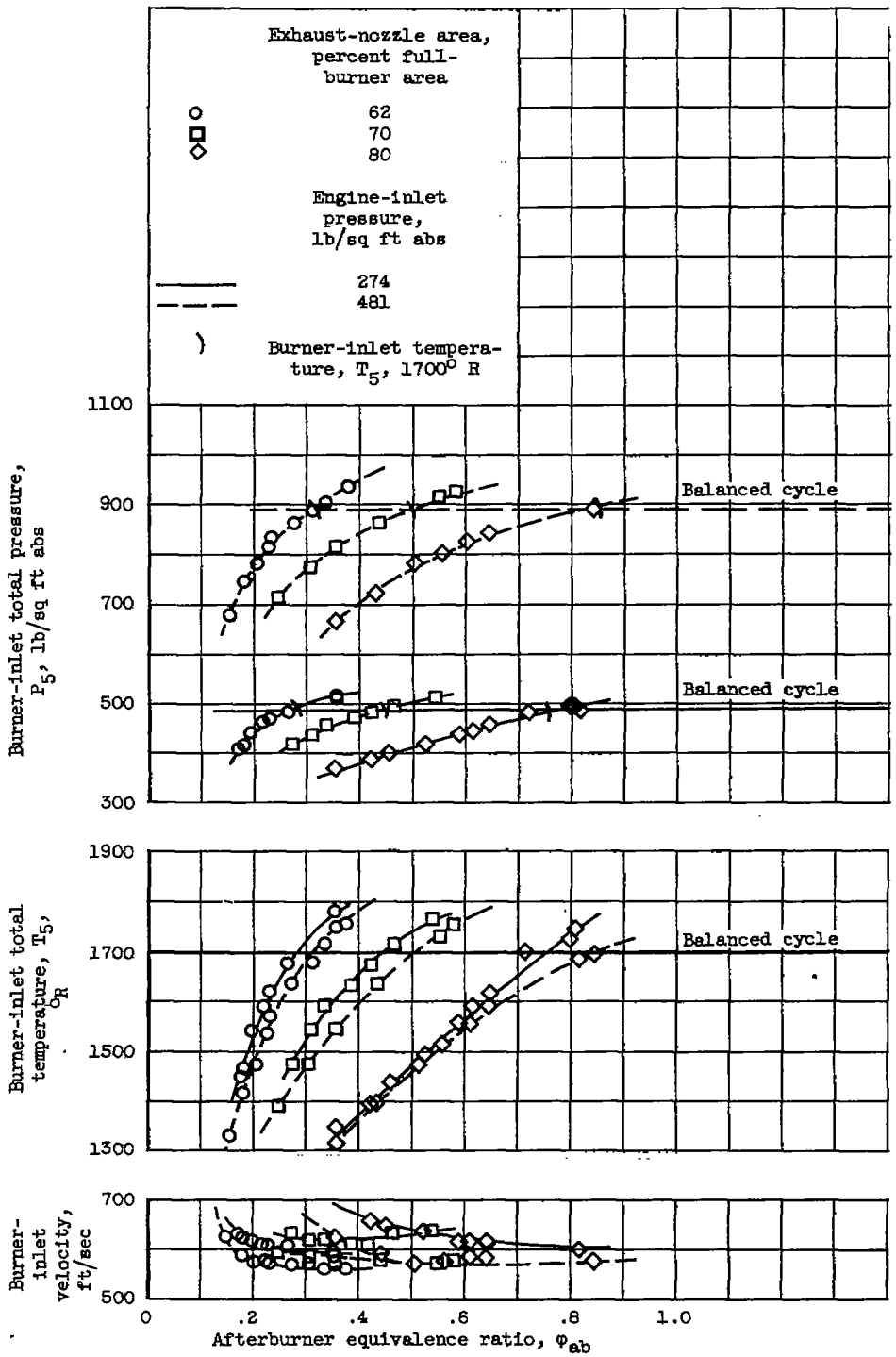

Figure 17. - Variations in burner environment and afterburner performance for three constant-area exhaust nozzles, fuel-ring configuration B. Burner length, 39 inches.

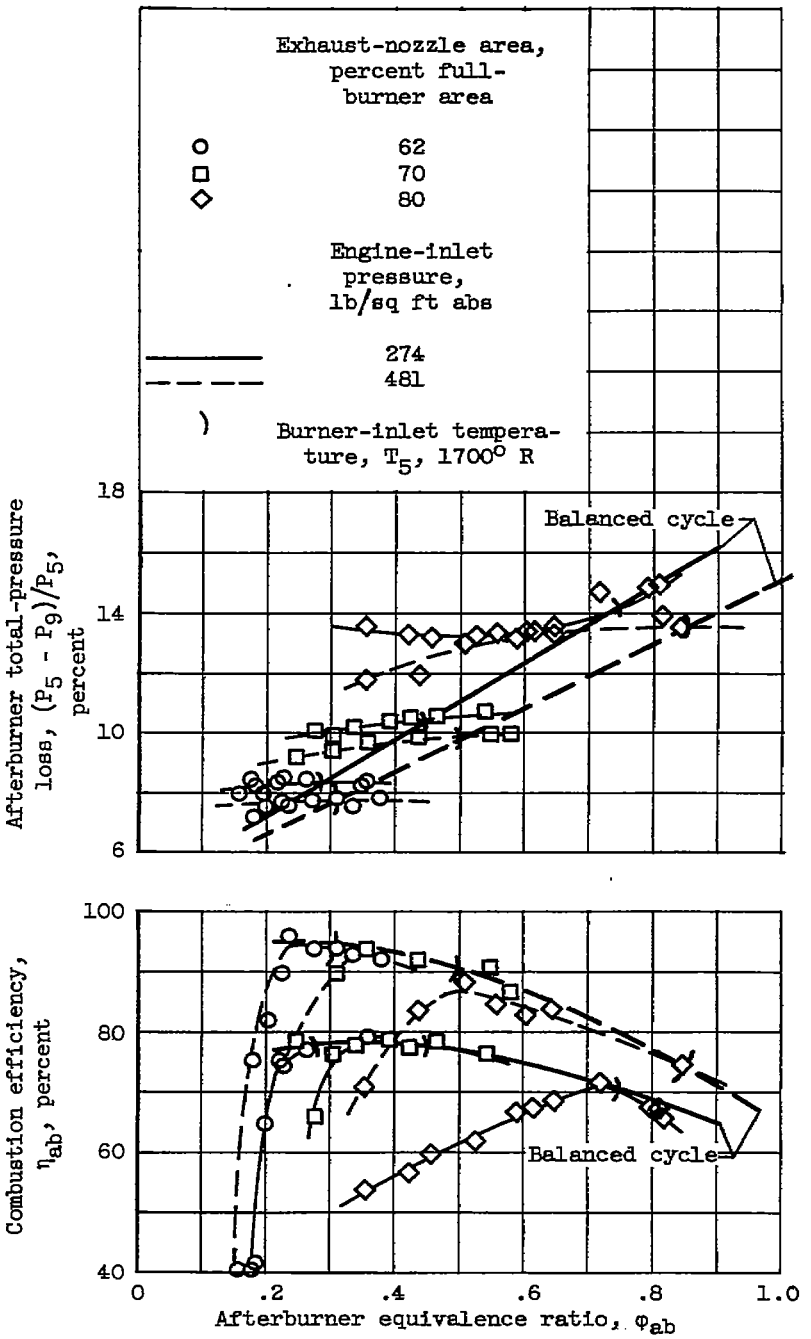

Figure 17. - Concluded. Variations in burner environment and afterburner performance for three constant-area exhaust nozzles, fuel-ring configuration B. Burner length, 39 inches.

[redacted]

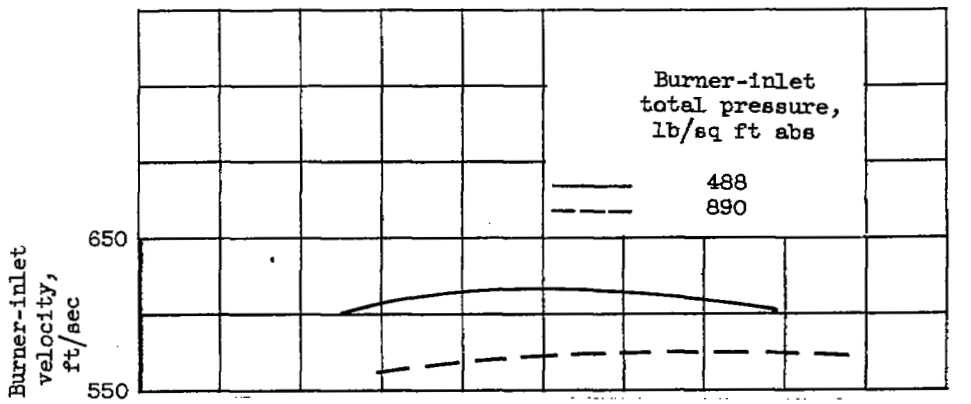

(a) Velocity.

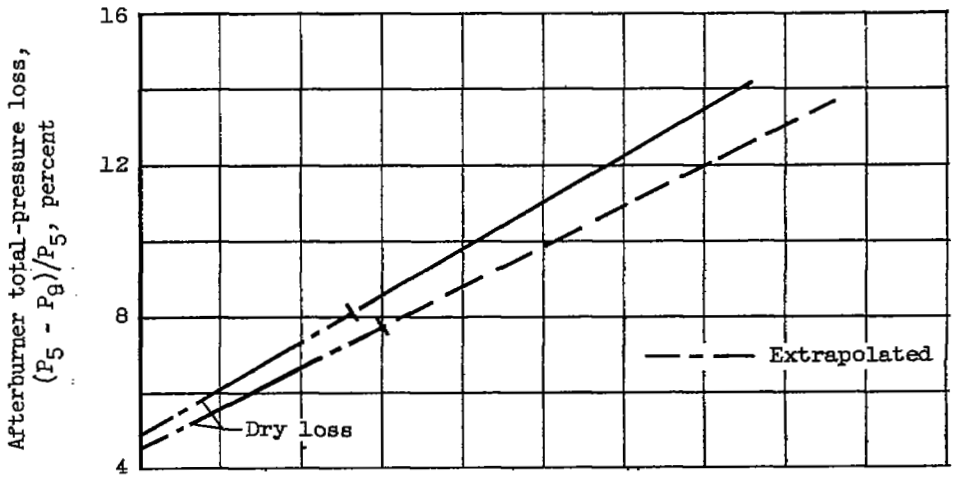

(b) Pressure loss.

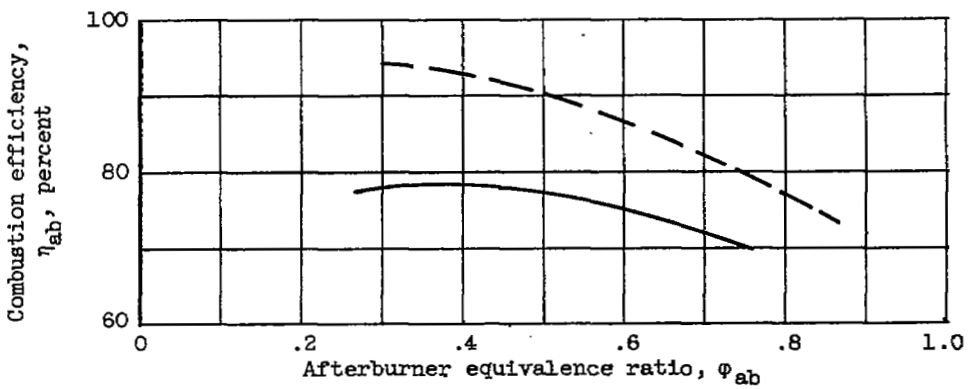

(c) Efficiency.

Figure 18. - Effect of burner pressure level on afterburner performance for balanced-cycle operation, fuel-ring configuration B. Burner length, 39 inches.

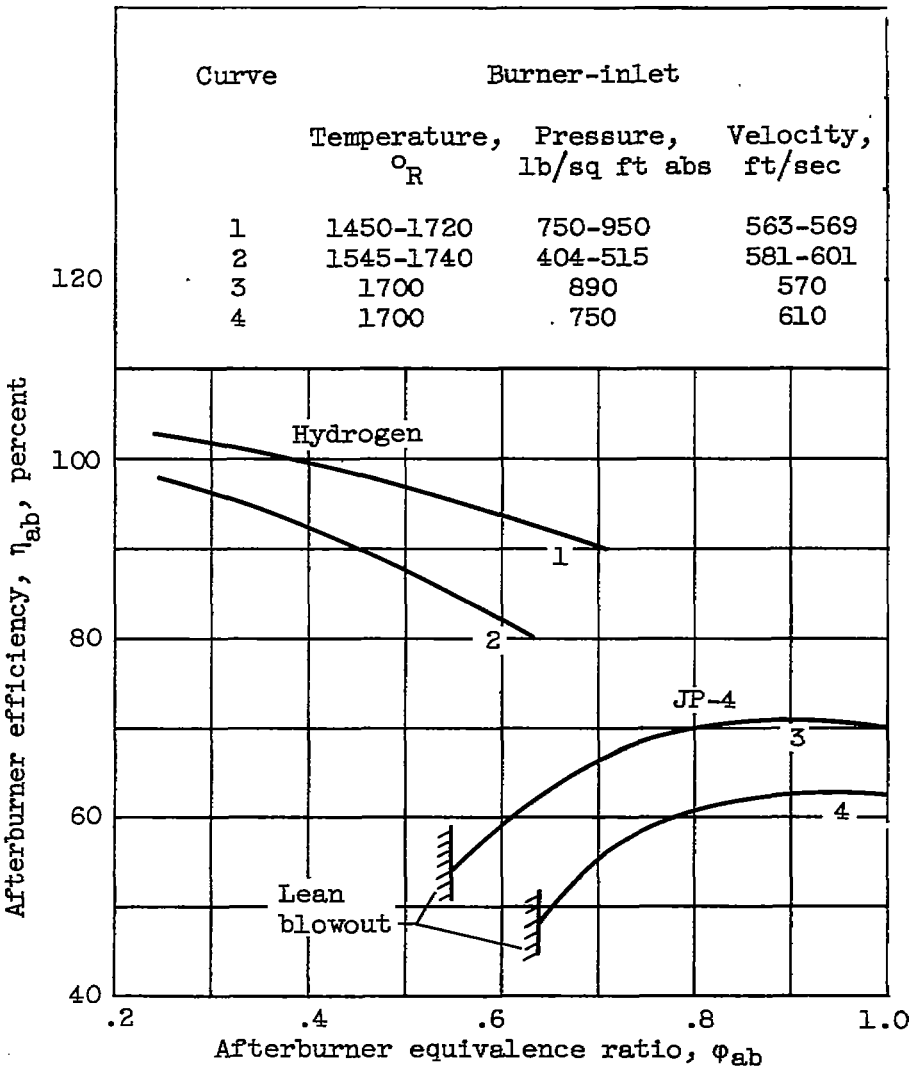

Figure 19. - Performance comparison of hydrogen and JP-4 fuels. Burner length, 39 inches; radial fuel-bar injectors.

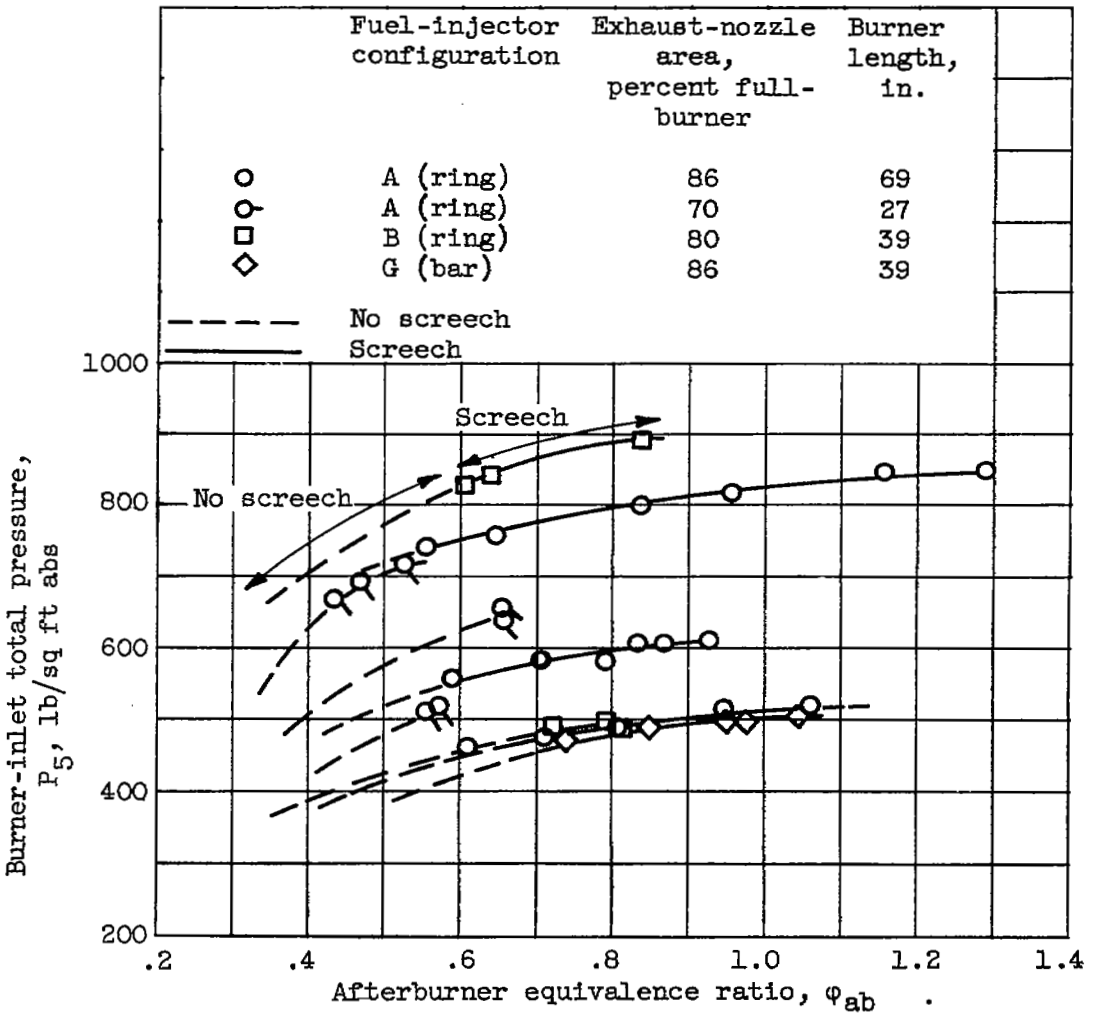

Figure 20. - Occurrence of audible screech at steady-state operating conditions as noted for all configurations investigated. (Data points represent operation in screech.)